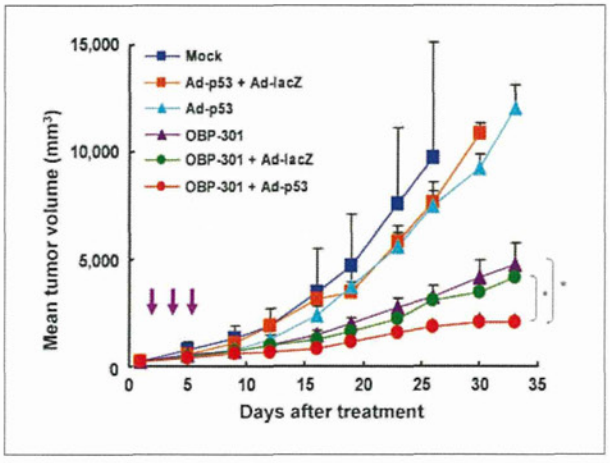

Figure 6. H1299 cells (7.5×10^6 cells/mouse) were injected s.c. into the flank of BALB/c *nu/nu* mice and permitted to grow to 4 to 10 mm in diameter. A 50 μL solution containing Ad-p53 (1×10^9 pfu), OBP-301 (1×10^7 pfu), OBP-301 (1×10^7 pfu) + Ad-p53 (1×10^8 pfu), or Ad-lacZ (1×10^8 pfu), Ad-p53 (1×10^8 pfu) + Ad-lacZ (1×10^7 pfu), or PBS was injected into the tumor for three cycles every 2 d. The perpendicular diameter of each tumor was measured every 3 or 4 d. Six or seven mice were used for each group. Points, mean tumor growth volume; bars, SE. *, $P < 0.05$, statistical significance (Student's *t* test). Arrows, days of treatment.

Discussion

Resistance to apoptosis is a major cause of treatment failure in human cancers. Many combination regimens with clinically available agents are currently being used; however, there is a need for a better understanding of the molecular interaction of drugs to efficiently induce apoptosis in human cancer cells. In the present study, our goal was to determine whether dual virotherapy, which mediates telomerase-specific enhancement of exogenous wild-type p53 gene expression, was effective for inducing apoptosis. We found that Ad-p53 and OBP-301, with different mechanisms of action, could be more effective in the growth of human cancer cells than Ad-p53 or OBP-301 alone *in vitro* as well as *in vivo*. Moreover, our data suggest that p53-induced p21 induction was inhibited in the presence of OBP-301 infection, which might in turn sensitize tumor cells to apoptosis by blocking cell cycle arrest.

Virotherapy for p53 gene transfer by Ad-p53 (Advexin) is currently in clinical trials as a cancer therapeutic (24). Overexpression of p53 gene caused preferential cancer cell–killing, although this was less toxic to normal cells, which means that p53 gene therapy itself is a cancer-targeting therapy; however, the low transduction rate and the narrow spread of Ad-p53 limits the anticancer effect *in vivo*. The major problem for p53 therapy with replication-defective adenovirus vector is incomplete transduction of target cancer cells. Therefore, cancer cells beyond transduced cells will escape the antitumor effect. To overcome the low transduction rate of replication-defective adenoviral vectors, an increment in the dose would be the simple resolution; however, a higher dose of Ad-p53 might not always contribute to the improvement of transduction efficacy and could potentially cause side effects. In this study, even the low dose of Ad-p53, administration of which solely was not enough to induce apoptosis, enabled an increase anticancer effect in combination with OBP-301 by replicating selectively in tumor cells. OBP-301 was genetically designed to replicate specifically in tumor cells, causing specific "oncolysis"(13, 15, 16), thereby increasing the effective treatment radius in tumors. This combination might contribute to the mitigation of unfavorable effects. OBP-301 is currently being evaluated in phase I trials for clinical safety as of the writing of this article.

Virotherapy with adenovirus Onyx-015, the first oncolytic virus, has been evaluated in clinical trials, and showed that administration of oncolytic adenovirus via intratumor, intraperitoneum, or intravenous methods was well tolerated (25); however, the efficacy of Onyx-015 as a single agent is also limited, possibly because of inefficient cell lysis and release of their progeny, which may be defective in cancer cells. Our strategy is aiming not only to enhance the antitumor activity of Ad-p53 by OBP-301, but also to augment the oncolytic activity of OBP-301 in combination with Ad-p53. Oncolysis is due to cytopathic effects intrinsic to the adenovirus. Adenovirus must be able to induce cell death in infected cells for the virus to generate a cytopathic effect and be released from the cell. Hall et al. showed that wild-type p53 enhances the ability of adenoviruses to induce cell death, whereas the loss of functional p53 in cancer cells resulted in a defect in adenovirus-induced cytopathic effects (26). Thus, functional p53 is required for a productive adenovirus infection. Consistent with their report, our strategy to compensate or overexpress functional wild-type p53 must be conducive to efficient adenovirus replication, which leads to effective oncolysis by OBP-301.

The efficacy of combination therapy with conventional gene therapy using replication-deficient adenovirus plus virotherapy has been reported previously (27, 28). Combined with tumor-specific replication-selective adenovirus, replication-deficient adenoviruses were able to replicate and spread to surrounding tumor cells. Antitumor activity was increased compared with gene therapy alone or virotherapy alone in agreement with our study. In our previous study, co-infection with a replication-deficient adenovirus expressing the green fluorescent protein (*GFP*) gene and OBP-301 was able to specifically visualize human lung cancer cells in an orthotopic murine model (14). Although the study showed the diagnostic application of combinative use of replication deficient adenoviral vector and OBP-301, the specific replication of coinfected adenovirus in tumor was visually evidenced. The current study applied this principle to therapeutic purpose. When Ad-p53 was used together with OBP-301, the total amount of the viruses might be higher than that of OBP-301 alone that shows the equivalent efficacy; the dose of replicative OBP-301, however, should be reduced as much as possible from the viewpoint of safety.

Indeed, the pharmacodynamic data in a phase I clinical trial of OBP-301 showed the transient systemic dissemination of OBP-301 following intratumoral injection (29).

Another interesting finding in the current study is that OBP-301 infection apparently inhibited exogenous p53-mediated expression of p21, which is a key player in arresting cells in the G_1 phase. This suggests that OBP-301 infection might be an important requirement for rendering tumor cells sensitive to apoptosis rather than cell cycle arrest. Indeed, it has been reported that the adenovirus E1A protein could enhance the sensitivity of tumor cells to chemotherapeutic agents by promoting apoptosis (30). This is primarily because of the ability of E1A to interact with p21 and thereby inactivate it, which in turn, leads to apoptosis. Further mechanisms of this interaction are now under investigation.

Our strategies aim to enhance the efficiency and specificity of viral agents through incorporation of tumor-targeting mechanisms via therapeutic gene and transcriptional regulation. Although this study examined the combinative use of two viral agents, oncolytic adenoviruses carrying therapeutic genes in the E1 or E3 region have also been reported (31, 32). Gene therapy and oncolytic virotherapy, however, do not always work effectively in combination (33). In case the expression level of therapeutic genes needs to be titrated, therapeutic genes might work better when separated from oncolytic virus. In addition, both p53 therapy and OBP-301 oncolytic therapy are currently being tested clinically. Once they are approved for clinical use, this study would provide realistic therapeutic applications as a preclinical study in the future.

In conclusion, our data showed that combination therapy of Ad-p53 and OBP-301 efficiently inhibited human cancer cell growth *in vitro* and *in vivo*, and that this approach has important implications for the treatment of human cancers.

Disclosure of Potential Conflicts of Interest

Y. Urata: employee of Oncolys BioPharma, Inc. T. Fujiwara: consultant to Oncolys BioPharma, Inc. No other potential conflicts of interest were disclosed.

Acknowledgments

We thank Daiju Ichimaru and Hitoshi Kawamura for their helpful discussions. We also thank Tomoko Sueishi for her excellent technical support.

Grant Support

Grants-in-Aid from the Ministry of Education, Science, and Culture, Japan (T. Fujiwara) and the Ministry of Health, Labour and Welfare, Japan (T. Fujiwara).

The costs of publication of this article were defrayed in part by the payment of page charges. This article must therefore be hereby marked *advertisement* in accordance with 18 U.S.C. Section 1734 solely to indicate this fact.

Received 06/19/2009; revised 03/26/2010; accepted 04/01/2010; published OnlineFirst 05/25/2010.

References

1. Grem JL. Biochemical modulation of 5-FU in systemic treatment of advanced colorectal cancer. Oncology (Williston Park) 2001;15: 13–9.
2. Kumar S, Gao L, Yeagy B, Reid T. Virus combinations and chemotherapy for the treatment of human cancers. Curr Opin Mol Ther 2008;10:371–9.
3. Senzer N, Mani S, Rosemurgy A, et al. TNFerade biologic, an adenovector with a radiation-inducible promoter, carrying the human tumor necrosis factor α gene: a phase I study in patients with solid tumors. J Clin Oncol 2004;22:592–601.
4. Hollstein M, Sidransky D, Vogelstein B, Harris CC. p53 mutations in human cancers. Science 1991;253:49–53.
5. Levine AJ, Perry ME, Chang A, et al. The 1993 Walter Hubert lecture: the role of the p53 tumour-suppressor gene in tumorigenesis. Br J Cancer 1994;69:409–16.
6. Swisher SG, Roth JA, Nemunaitis J, et al. Adenovirus-mediated p53 gene transfer in advanced non-small-cell lung cancer. J Natl Cancer Inst 1999;91:763–71.
7. Nemunaitis J, Swisher SG, Timmons T, et al. Adenovirus-mediated p53 gene transfer in sequence with cisplatin to tumors of patients with non-small-cell lung cancer. J Clin Oncol 2000;18:609–22.
8. Swisher SG, Roth JA, Komaki R, et al. Induction of p53-regulated genes and tumor regression in lung cancer patients after intratumoral delivery of adenoviral p53 (INGN 201) and radiation therapy. Clin Cancer Res 2003;9:93–101.
9. Fujiwara T, Tanaka N, Kanazawa S, et al. Multicenter phase I study of repeated intratumoral delivery of adenoviral p53 in patients with advanced non-small-cell lung cancer. J Clin Oncol 2006;24: 1689–99.
10. Bischoff JR, Kirn DH, Williams A, et al. An adenovirus mutant that replicates selectively in p53-deficient human tumor cells. Science 1996;274:373–6.
11. Rodriguez R, Schuur ER, Lim HY, Henderson GA, Simons JW, Henderson DR. Prostate attenuated replication competent adenovirus (ARCA) CN706: a selective cytotoxic for prostate-specific antigen-positive prostate cancer cells. Cancer Res 1997;57: 2559–63.
12. Kirn D, Martuza RL, Zwiebel J. Replication-selective virotherapy for cancer: biological principles, risk management and future directions. Nat Med 2001;7:781–7.
13. Kawashima T, Kagawa S, Kobayashi N, et al. Telomerase-specific replication-selective virotherapy for human cancer. Clin Cancer Res 2004;10:285–92.
14. Umeoka T, Kawashima T, Kagawa S, et al. Visualization of intrathoracically disseminated solid tumors in mice with optical imaging by telomerase-specific amplification of a transferred green fluorescent protein gene. Cancer Res 2004;64:6259–65.
15. Taki M, Kagawa S, Nishizaki M, et al. Enhanced oncolysis by a tropism-modified telomerase-specific replication-selective adenoviral agent OBP-405 ('Telomelysin-RGD'). Oncogene 2005;24:3130–40.
16. Fujiwara T, Kagawa S, Kishimoto H, et al. Enhanced antitumor efficacy of telomerase-selective oncolytic adenoviral agent OBP-401 with docetaxel: preclinical evaluation of chemovirotherapy. Int J Cancer 2006;119:432–40.
17. Kishimoto H, Kojima T, Watanabe Y, et al. *In vivo* imaging of lymph node metastasis with telomerase-specific replication-selective adenovirus. Nat Med 2006;12:1213–9.
18. Blackburn EH. Structure and function of telomeres. Nature 1991;350: 569–73.
19. Kim NW, Piatyszek MA, Prowse KR, et al. Specific association of

human telomerase activity with immortal cells and cancer. Science 1994;266:2011–5.
20. Shay JW, Wright WE. Telomerase activity in human cancer. Curr Opin Oncol 1996;8:66–71.
21. Nakayama J, Tahara H, Tahara E, et al. Telomerase activation by hTRT in human normal fibroblasts and hepatocellular carcinomas. Nat Genet 1998;18:65–8.
22. Fujiwara T, Tanaka N, Numunaitis JJ, et al. Phase I trial of intratumoral administration of OBP-301, a novel telomerase-specific oncolytic virus, in patients with advanced solid cancer: evaluation of biodistribution and immune response. J Clin Oncol 2008;26:3572.
23. Ohtani S, Kagawa S, Tango Y, et al. Quantitative analysis of p53-targeted gene expression and visualization of p53 transcriptional activity following intratumoral administration of adenoviral p53 *in vivo*. Mol Cancer Ther 2004;3:93–100.
24. Roth JA. Adenovirus p53 gene therapy. Expert Opin Biol Ther 2006; 6:55–61.
25. Kirn D. Oncolytic virotherapy for cancer with the adenovirus dl1520 (Onyx-015): results of phase I and II trials. Expert Opin Biol Ther 2001;1:525–38.
26. Hall AR, Dix BR, O'Carroll SJ, Braithwaite AW. p53-dependent cell death/apoptosis is required for a productive adenovirus infection. Nat Med 1998;4:1068–72.
27. Lee CT, Lee YJ, Kwon SY, et al. *In vivo* imaging of adenovirus transduction and enhanced therapeutic efficacy of combination therapy with conditionally replicating adenovirus and adenovirus-p27. Cancer Res 2006;66:372–7.
28. Li X, Raikwar SP, Liu YH, et al. Combination therapy of androgen-independent prostate cancer using a prostate restricted replicative adenovirus and a replication-defective adenovirus encoding human endostatin-angiostatin fusion gene. Mol Cancer Ther 2006;5:676–84.
29. Nemunaitis J, Tong AW, Nemunaitis M, et al. A phase I study of telomerase-specific replication competent oncolytic adenovirus (telomelysin) for various solid tumors. Mol Ther 2010;18: 429–34.
30. Chattopadhyay D, Ghosh MK, Mal A, Harter ML. Inactivation of p21 by E1A leads to the induction of apoptosis in DNA-damaged cells. J Virol 2001;75:9844–56.
31. Haviv YS, Takayama K, Glasgow JN, et al. A model system for the design of armed replicating adenoviruses using p53 as a candidate transgene. Mol Cancer Ther 2002;1:321–8.
32. Nanda D, Vogels R, Havenga M, Avezaat CJ, Bout A, Smitt PS. Treatment of malignant gliomas with a replicating adenoviral vector expressing herpes simplex virus-thymidine kinase. Cancer Res 2001; 61:8743–50.
33. Hioki M, Kagawa S, Fujiwara T, et al. Combination of oncolytic adenovirotherapy and Bax gene therapy in human cancer xenografted models. Potential merits and hurdles for combination therapy. Int J Cancer 2008;122:2628–33.

Therapeutics, Targets, and Chemical Biology

Cancer Research

Telomerase-Dependent Oncolytic Adenovirus Sensitizes Human Cancer Cells to Ionizing Radiation via Inhibition of DNA Repair Machinery

Shinji Kuroda[1], Toshiya Fujiwara[1], Yasuhiro Shirakawa[1], Yasumoto Yamasaki[1], Shuya Yano[1], Futoshi Uno[1], Hiroshi Tazawa[2], Yuuri Hashimoto[1], Yuichi Watanabe[1,3], Kazuhiro Noma[1], Yasuo Urata[3], Shunsuke Kagawa[1], and Toshiyoshi Fujiwara[1,2]

Abstract

The inability to repair DNA double-strand breaks (DSB) leads to radiosensitization, such that ionizing radiation combined with molecular inhibition of cellular DSB processing may greatly affect treatment of human cancer. As a variety of viral products interact with the DNA repair machinery, oncolytic virotherapy may improve the therapeutic window of conventional radiotherapy. Here, we describe the mechanistic basis for synergy of irradiation and OBP-301 (Telomelysin), an attenuated type-5 adenovirus with oncolytic potency that contains the human telomerase reverse transcriptase promoter to regulate viral replication. OBP-301 infection led to E1B55kDa viral protein expression that degraded the complex formed by Mre11, Rad50, and NBS1, which senses DSBs. Subsequently, the phosphorylation of cellular ataxia-telangiectasia mutated protein was inhibited, disrupting the signaling pathway controlling DNA repair. Thus, tumor cells infected with OBP-301 could be rendered sensitive to ionizing radiation. Moreover, by using noninvasive whole-body imaging, we showed that intratumoral injection of OBP-301 followed by regional irradiation induces a substantial antitumor effect, resulting from tumor cell–specific radiosensitization, in an orthotopic human esophageal cancer xenograft model. These results illustrate the potential of combining oncolytic virotherapy and ionizing radiation as a promising strategy in the management of human cancer. *Cancer Res; 70(22); 9339–48. ©2010 AACR.*

Introduction

Current treatment strategies for advanced cancer include surgical resection, radiation, and cytotoxic chemotherapy. Preoperative or postoperative chemoradiation may improve local control and the survival of advanced cancer patients by minimizing the risk of dissemination during the surgical procedure, increasing the complete resection rate, and eradicating microscopic residual tumor cells that are not surgically removed. The lack of restricted selectivity for tumor cells is the primary limitation of radiotherapy, despite improved technologies such as stereotactic and hyperfractionated radiotherapy. Although radiotherapy is generally considered to be less invasive, the maximum doses and treatment fields are limited to avoid the influence on the surrounding normal tissues. Therefore, to improve the therapeutic index of radiotherapy while maintaining a tolerance of normal tissue toxicity, there is a need for agents that effectively lower the threshold for radiation-induced tumor cell death; the safety and efficacy of some candidates are already being explored in clinical trials (1–3).

Ionizing radiation primarily targets DNA molecules and induces double-strand breaks (DSB; ref. 4). Radiosensitization can result from a therapeutic increase in DNA DSBs or inhibition of their repair. Ataxia-telangiectasia mutated (ATM) protein is an important signal transducer of the DNA damage response, which contains DNA repair and cell cycle checkpoints, and activation of ATM by autophosphorylation occurs in response to exposed DNA DSBs (5). Cells mutated in the ATM gene have defects in cell cycle checkpoints and DNA repair and are hypersensitive to DSBs (6, 7); thus, agents that inhibit the ATM pathway can be useful radiosensitizers (8). The Mre11, Rad50, and NBS1 (MRN) complex is quickly stimulated by DSBs and directly activates ATM (9, 10). Defects in the MRN complex lead to genomic instability, telomere shortening, and hypersensitivity to DNA damage (11).

We reported previously that telomerase-specific, replication-selective adenovirus (Telomelysin, OBP-301), in which the human telomerase reverse transcriptase (hTERT) promoter element drives the expression of *E1* genes, induced selective

Authors' Affiliations: [1]Department of Gastroenterological Surgery, Okayama University Graduate School of Medicine, Dentistry and Pharmaceutical Sciences; [2]Center for Gene and Cell Therapy, Okayama University Hospital, Okayama, Japan; and [3]Oncolys BioPharma, Inc., Tokyo, Japan

Note: Supplementary data for this article are available at Cancer Research Online (http://cancerres.aacrjournals.org/).

Corresponding Author: Toshiyoshi Fujiwara, Department of Gastroenterological Surgery, Okayama University Graduate School of Medicine, Dentistry and Pharmaceutical Sciences, 2-5-1 Shikata-cho, Kita-ku, Okayama 700-8558, Japan. Phone: 81-86-235-7257; Fax: 81-86-221-8775; E-mail: toshi_f@md.okayama-u.ac.jp.

doi: 10.1158/0008-5472.CAN-10-2333

E1 expression, and efficiently killed human cancer cells but not normal human somatic cells (12–15). Adenoviral E1B55kDa protein, a gene product in the adenoviral early region, inhibits the functions of p53 and the MRN complex by cooperating with adenoviral E4orf6 protein, leading to the proteolytic degradation of these proteins (10, 16–18). In the present study, we showed the synergistic efficacy of combined treatment with ionizing radiation and OBP-301 against human cancer cells, and we clarified the E1B55kDa-mediated mechanism used by OBP-301 to inhibit DNA repair.

Materials and Methods

Cell lines and cell cultures

The human non–small-cell lung cancer cell line A549 was propagated in DMEM containing Nutrient Mixture (Ham's F-12) and supplemented with 10% FCS. The human esophageal squamous cell carcinoma cell line TE8 was cultured in RPMI 1640 supplemented with 10% FCS. The human esophageal adenocarcinoma cell line SEG1 was cultured in DMEM supplemented with 10% FCS. TE8 cells transfected with the firefly luciferase plasmid vector (TE8-Luc) were maintained in medium containing 0.2 mg/mL Geneticin (G418).

Adenovirus

The recombinant, replication-selective, tumor-specific adenovirus vector OBP-301 (Telomelysin), in which the hTERT promoter element drives the expression of *E1A* and *E1B* genes linked with an internal ribosome entry site, was previously characterized (12–15). The wild-type adenovirus type 5 (Ad-wt) and the E1B55kDa-defective adenovirus mutant dl1520 (Onyx-015) were also used (19).

Cell viability assay

A549, TE8, and SEG1 cells were infected with OBP-301 at the indicated multiplicities of infection (MOI) and then irradiated at the indicated dosages by using an MBR-1520R device (Hitachi Medical Co.). Cell viability was determined 5 days after irradiation with a Cell Proliferation Kit II (Roche Molecular Biochemicals), according to the manufacturer's protocol. Synergy between radiation and OBP-301 was analyzed with the CalcuSyn software (BioSoft), and the computation of the combination index was based on the methods of Chou and Talalay (20).

Flow cytometry

Cells were incubated for 20 minutes on ice in Cytofix/Cytoperm solution (BD Biosciences) and labeled with phycoerythrin (PE)-conjugated rabbit monoclonal active caspase-3 antibody (BD Biosciences) for 30 minutes and analyzed by FACSArray (BD Biosciences).

Immunofluorescence staining

Cells seeded on tissue culture chamber slides were treated and then fixed with cold methanol for 30 minutes on ice. The slides were subsequently incubated with primary antibody against pATM (Rockland), Mre11, Rad50 (GeneTex), NBS1 (Novus), and E1B55kDa (kindly provided by Dr. Arnold Levine, The Institute for Advanced Study, Princeton, NJ) for 1 hour on ice. After washing twice with PBS, slides were incubated with the secondary antibody, FITC-conjugated rabbit anti-mouse IgG (Zymed Laboratories), FITC-conjugated goat anti-rabbit IgG (Vector Laboratories), or Alexa 568–conjugated goat anti-mouse IgG (Molecular Probes), for 1 hour on ice. The slides were further stained with 4′,6-diamidino-2-phenylindole, mounted by using Fluorescent Mounting Medium (Dako Cytomation), and then analyzed with an LSM510 confocal laser microscope (Zeiss).

Western blot analysis

The primary antibodies against pATM (Cell Signaling), ATM (Novus), Mre11, Rad50, NBS1, E1B55kDa (kindly provided by Dr. Levine), γH2AX (Upstate), poly(ADP-ribose) polymerase (PARP; Cell Signaling), β-actin (Sigma), and peroxidase-linked secondary antibodies (Amersham) were used. Proteins were electrophoretically transferred to Hybond-polyvinylidene difluoride transfer membranes (GE Healthcare Life Science) and incubated with primary antibody, followed by peroxidase-linked secondary antibody. The Amersham ECL chemiluminescence system (GE Healthcare Life Science) was used to detect the peroxidase activity of the bound antibody.

In vivo subcutaneous human tumor model

A549, TE8, and SEG1 cells (2×10^6 per mouse) were injected s.c. into the flanks of 5- to 6-week-old female BALB/c *nu/nu* mice. When tumors reached ~3 to 5 mm in diameter, the mice were irradiated at a dosage of 3 Gy/tumor every 2 days (for A549) or 2 Gy/tumor every week (for TE8 and SEG1) for three cycles starting at day 0. When irradiated, mice were placed prone in custom-made holders that contain lead collimators to shield the upper half of the mice. Immediately after radiation, OBP-301 at a dose of 1×10^8 plaque-forming units (PFU)/tumor or PBS was injected into the tumor. In experiments with larger tumors, subcutaneous TE8 tumors with a diameter of 8 to 10 mm were treated with radiation at 2 Gy/tumor and intratumoral injection of OBP-301 at 1×10^8 PFU/tumor three times per week (every 2 days) for three cycles (nine times in total). The perpendicular diameter of each tumor was measured every 3 to 4 days, and tumor volume was calculated with the following formula: tumorvolume (mm^3) = $a \times b^2 \times 0.5$, where a is the longest diameter, b is the shortest diameter, and 0.5 is a constant to calculate the volume of an ellipsoid. The experimental protocol was approved by the Ethics Review Committee for Animal Experimentation of Okayama University.

Orthotopic human esophageal cancer model

TE8-Luc cells (2×10^6 per mouse) suspended in Matrigel were inoculated into the abdominal esophagus of 6-week-old female BALB/c *nu/nu* mice during laparotomy. Three weeks later, mice were irradiated with 2 Gy/tumor in holders that contain lead collimators to shield the head, neck, and chest of the mice. Immediately after radiation, mice were intratumorally injected with OBP-301 at 1×10^8 PFU/tumor during laparotomy, every 2 days for three cycles. To monitor tumor progression, the substrate luciferin was injected i.p. at a dose

of 150 mg/kg body weight. Images were collected in the supine position every few minutes from 10 to 30 minutes after luciferin injection with the IVIS Imaging System (Xenogen), and photons emitted from the abdominal esophagus region were quantified by using Living Image Software (Xenogen).

Statistical analysis

All data were expressed as mean ± SD. Differences between groups were examined for statistical significance with the Student's *t* test. *P* values <0.05 were considered statistically significant.

Results

Radiosensitizing effect of OBP-301 *in vitro*

To examine the potential interaction between OBP-301 and ionizing radiation *in vitro*, we first evaluated their combined effect in human lung (A549) and esophageal (TE8 and SEG1) cancer cell lines. The cells received a single dose of ionizing irradiation 24 hours after either mock or OBP-301 infection, and the cell viability was assessed by 2,3-bis[2-methoxy-4-nitro-*S*-sulfophenynl]*H*-tetrazolium-5-carboxanilide inner salt (XTT) assay 5 days after irradiation. The addition of OBP-301 increased the cytotoxicity of ionizing radiation in a dose-dependent manner. The combination index showed potent, statistically significant synergy between OBP-301 and radiation in all three cell lines (Fig. 1A). In contrast, synergy was not observed in normal human lung fibroblasts (NHLF) because the viral replication of OBP-301 was attenuated in telomerase-negative normal cells (Supplementary Fig. S2A, B).

We measured the amount of apoptosis in A549 and TE8 cells that were irradiated after OBP-301 infection. The cells were infected with OBP-301 at a MOI of 1.0, irradiated with a dose of 10 Gy 24 hours after infection, and analyzed for apoptosis. OBP-301 caused a significant increase in active caspase-3–positive cells in response to ionizing irradiation (Fig. 1B). Western blot analysis showed that ionizing radiation promoted the cleavage of PARP, a caspase-3 substrate and a biochemical marker of apoptosis, with prior OBP-301 infection (Fig. 1C). Moreover, OBP-301 infection before irradiation significantly increased the number of A549 cells with apoptotic nuclear morphology (Fig. 1D and E). Thus, OBP-301 combined with ionizing radiation synergistically increased the amount of apoptosis.

Degradation of the MRN complex by adenoviral E1B55kDa protein

To elucidate the molecular mechanism responsible for the synergy between OBP-301 and ionizing radiation, we examined the physical interaction between viral proteins and the MRN complex, which drives the DNA repair pathway as a sensor of DNA DSBs, through a series of confocal microscopy experiments. Immunofluorescence staining of A549 cells infected with OBP-301 at an MOI of 10 showed colocalization of the signals representing Mre11, NBS1, and Rad50, suggesting that these proteins exist as a complex. Moreover, there was marked overlap in the nuclear signals corresponding to adenoviral E1B55kDa and NBS1, indicating a direct interaction between the E1B55kDa protein and the MRN complex (Fig. 2A). Western blot analysis showed that the levels of Mre11, NBS1, and Rad50 protein gradually decreased after OBP-301 infection at an MOI of 10, as the E1B55kDa expression increased (Fig. 2B). The expression of the MRN complex remained unchanged in NHLF because E1B55kDa expression was absent after OBP-301 infection (Supplementary Fig. S2C).

To confirm the effect of adenoviral E1B55kDa on the MRN degradation, we compared the subcellular localization and degradation of Mre11 protein after infection with wild-type adenovirus (Ad-wt), an adenovirus mutant that lacked E1B55kDa (dl1520, Onyx-015), or OBP-301 in A549 cells. The Mre11 protein accumulated in the nucleus in a scattered pattern within 24 hours after OBP-301 or Ad-wt infection and then relocated to the perinuclear area and was degraded; however, the scattered nuclear signals of Mre11 remained largely undegraded 72 hours after dl1520 infection (Fig. 2C). We measured the proportions of the cells with each staining pattern (scattered, perinuclear, or degraded) to compare the subcellular dynamics of the Mre11 protein. OBP-301 and Ad-wt infection caused a rapid decrease in Mre11-positive cells compared with dl1520 infection (Fig. 2D and E), suggesting that the E1B55kDa protein is essential for the degradation of the MRN complex.

Inhibition of radiation-induced DNA damage responses by OBP-301

The MRN complex functions as a DSB sensor that activates the ATM-dependent signaling pathway, which coordinates cell cycle arrest with DNA repair. To further investigate the relationship between E1B55kDa and ATM activation, we examined the effect of OBP-301 infection on the radiation-induced phosphorylation of ATM (pATM) in A549 cells. Immunofluorescence analysis revealed spot signals of pATM throughout the nuclei 30 minutes after ionizing radiation; however, OBP-301 or Ad-wt infection (10 MOI) 24 hours before irradiation blocked the formation of pATM foci (Fig. 3A). Pretreatment with OBP-301 significantly reduced the number of pATM-positive cells compared with pretreatment with dl1520 lacking E1B55kDa (Fig. 3B). Western blot analysis also showed that ionizing radiation induced the phosphorylation of ATM, whereas expression of E1B55kDa by OBP-301 infection led to the degradation of the MRN complex, which was accompanied by a greatly reduced level of pATM (Fig. 3C). Following dl1520 infection, ATM phosphorylation was seen in the absence of E1B55kDa expression and MRN degradation.

We also investigated whether OBP-301 infection could abrogate the DNA repair process by using γH2AX, which is a sensitive indicator of DSBs. Ionizing radiation induced γH2AX expression as early as 30 minutes after treatment in both mock- and OBP-301–infected A549 cells. The levels of γH2AX protein gradually decreased as the DNA DSBs were repaired in mock-infected cells, but remained elevated in cells infected with OBP-301 24 hours before irradiation (Fig. 3D). Densitometric quantification revealed that the relative density of γH2AX/β-actin at 3 hours after irradiation decreased by 64% without prior OBP-301 infection, but decreased by only

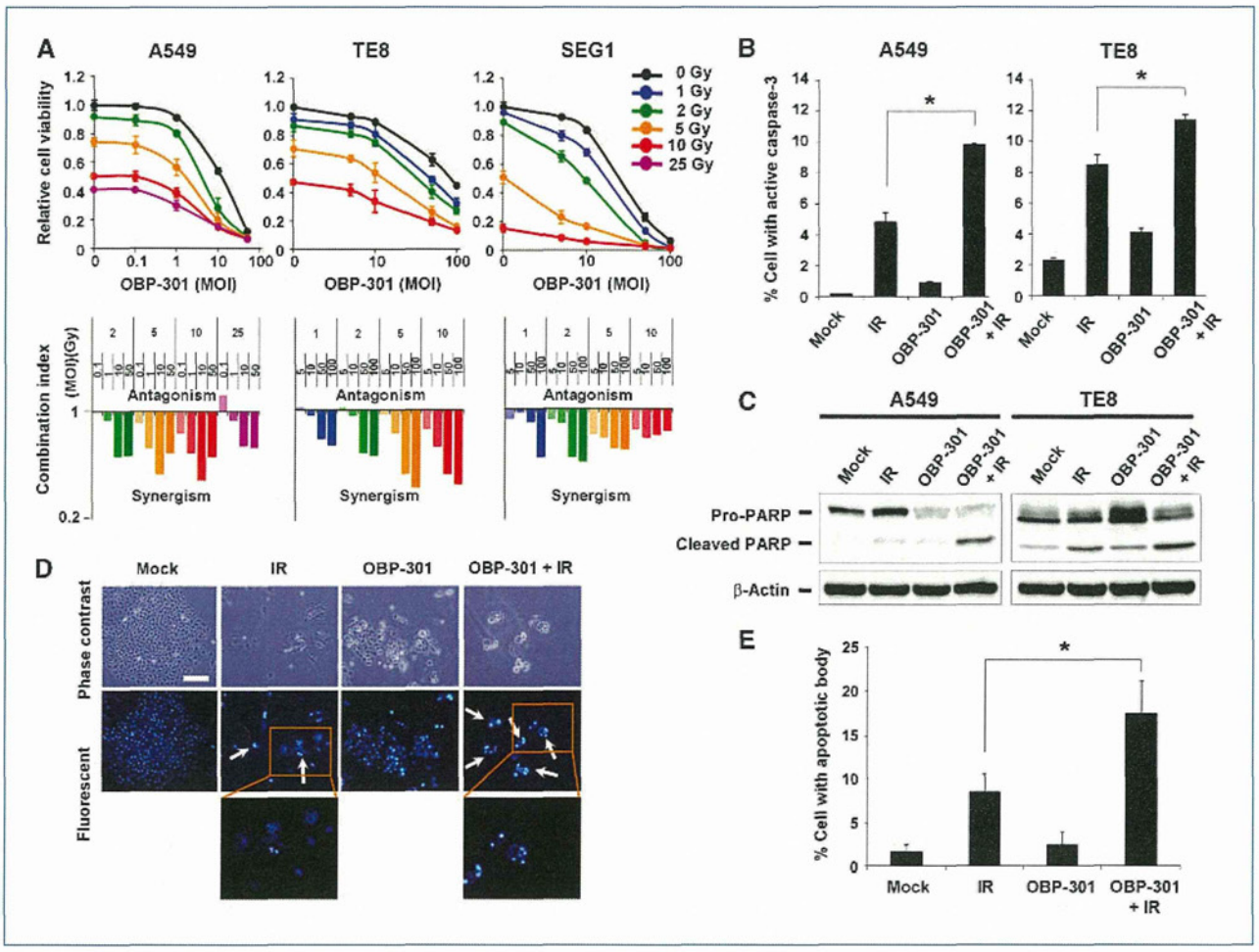

Figure 1. Radiosensitizing effect of OBP-301 on human cancer cells *in vitro*. A, cells were irradiated with the indicated doses 24 h after infection with OBP-301 at the indicated MOIs, and cell viability was assessed by XTT assay 5 d after irradiation. Top panels, percentages of viable cells relative to mock-treated cells. Error bars indicate 95% confidence intervals for triplicate data points. Bottom panels, the combination index was calculated with the CalcuSyn software. Synergy and antagonism were defined as interaction indices of <1 and >1, respectively. B to E, induction of apoptotic cell death by OBP-301 plus ionizing radiation. A549 and TE8 cells were infected with OBP-301 at an MOI of 1, irradiated with 10 Gy 24 h after infection, and then collected 5 d after irradiation. B, flow cytometric analysis for active caspase-3 expression. Cells were stained with PE-conjugated rabbit monoclonal active caspase-3 antibody and analyzed by FACS. *, $P < 0.01$. C, Western blot analysis for the cleavage of PARP. Blots were probed with anti-PARP antibody and visualized by using an ECL detection system. D, visualization of apoptotic nuclei. Treated A549 cells were stained with Hoechst 33342 and analyzed for DNA fragmentation by fluorescent microscopy. White arrows indicate cells with apoptotic bodies. The bottom panels are the magnified views of the boxed region in the middle panels. IR, ionizing radiation. E, the percentage of apoptotic cells was calculated by counting the number of cells with apoptotic bodies per 100 cells in six random fields in each group.

19% with OBP-301 infection compared with the levels at 30 minutes postirradiation (Fig. 3E). These results indicate that OBP-301 infection interrupts the cellular DNA repair mechanism induced by ionizing radiation.

Synergistic antitumor activity of OBP-301 plus radiation in human tumor xenografts

We next assessed the therapeutic efficacy of OBP-301 in combination with ionizing radiation against A549, TE8, and SEG1 cells *in vivo*. To determine the treatment schedule, we examined whether radiation could modify adenoviral infectivity and replication in human cancer cells. OBP-301 infection following ionizing radiation showed synergistic antitumor effects *in vitro* (Supplementary Fig. S3) due to an increased expression density of coxsackievirus and adenovirus receptor, which resulted in enhanced adenoviral uptake in human cancer cells (Supplementary Figs. S4 to S6). We also confirmed that ionizing radiation does not interfere with OBP-301 replication (Supplementary Fig. S7).

Based on these preliminary results, we chose a therapy regimen with three cycles of regional radiation followed immediately by intratumoral administration of OBP-301. Mice bearing A549, TE8, and SEG1 subcutaneous tumors that were 3 to 5 mm in diameter received 3 Gy (for A549) or 2 Gy (for TE8 and SEG1) local irradiation followed by the intratumoral injection of either 1×10^8 PFU of OBP-301 or PBS every 2 days (for A549) or 7 days (for TE8 and SEG1) for three cycles. Intratumoral administration of OBP-301 or radiation

alone resulted in significant tumor growth suppression compared with mock-treated tumors. The combination of OBP-301 plus radiation produced a more profound and significant inhibition of tumor growth compared with either modality alone in all three types of tumors, despite the difference in treatment schedules (Fig. 4A).

Histopathologic analysis of A549 tumors excised 10 days after the completion of three cycles of either regional radiation or OBP-301 infection revealed the degeneration of tissues and reduced tumor cell density compared with untreated tumors. However, treatment with OBP-301 injection plus radiation yielded massive tissue destruction and further reduction in tumor cell density. Moreover, the cytolytic changes induced by the combination therapy led to the development of hyalinized acellular stroma (Fig. 4B). Terminal deoxyribonucleotidyl transferase-mediated dUTP nick end labeling (TUNEL) staining showed that combining ionizing radiation with OBP-301 markedly increased the amount of apoptotic cells in A549 tumors excised 3 days after the completion of the treatment (Fig. 4C). OBP-301 plus irradiation apparently increased PARP cleavage in A549 tumors compared with ionizing radiation alone (Fig. 4D).

Eradication of established human tumor xenografts by OBP-301 plus radiation

To mimic the clinical characteristics of advanced cancer patients, we established TE8 xenografts with a 10-fold larger tumor burden. Mice bearing large TE8 subcutaneous tumors received nine cycles of 2 Gy irradiation followed by intratumoral injection of 1×10^8 PFU of OBP-301 three times per week for 3 weeks. Tumors treated with either OBP-301 or ionizing radiation alone exhibited a transient shrinkage,

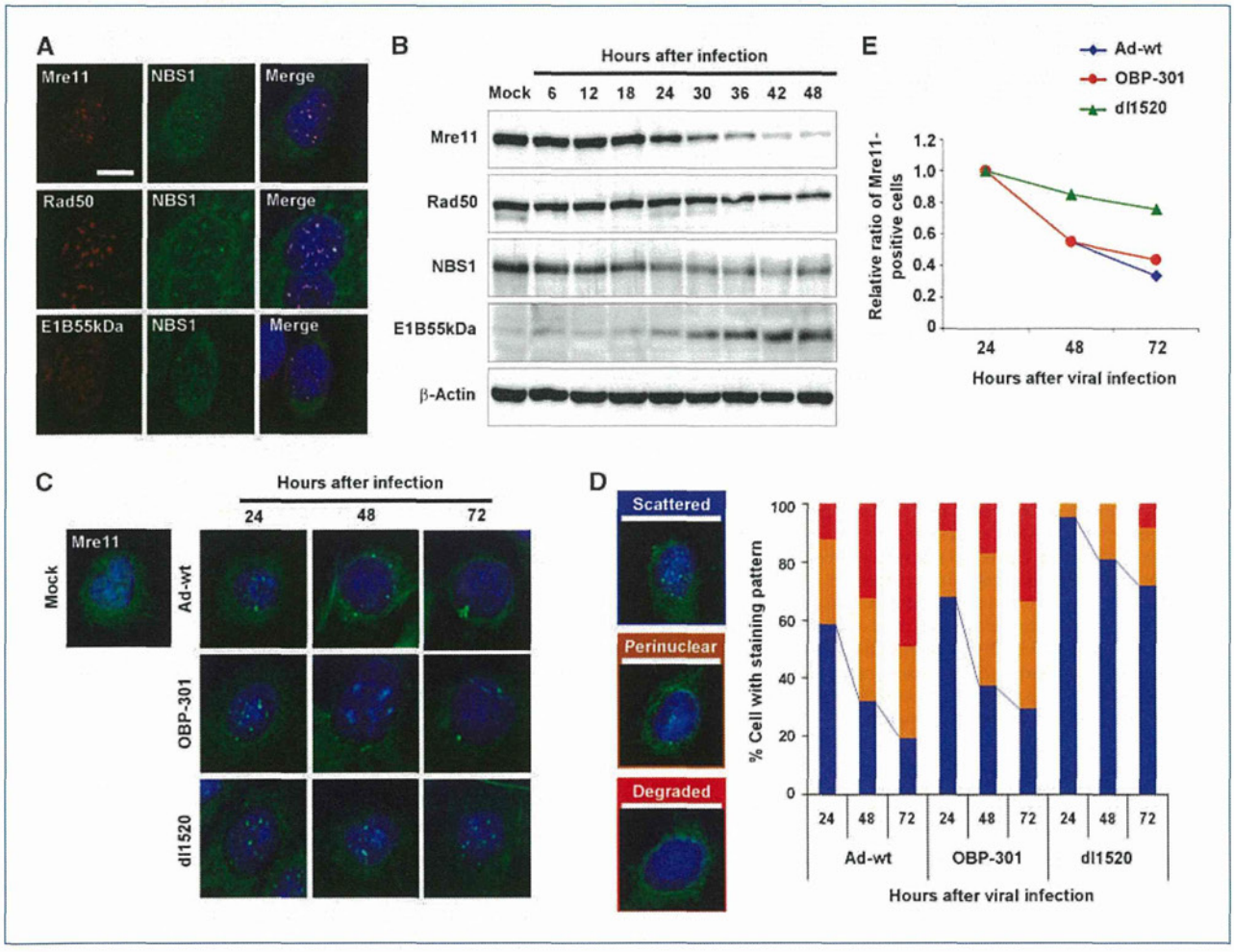

Figure 2. Degradation of the MRN complex by E1B55kDa protein. A, A549 cells were infected with OBP-301 at an MOI of 10 and then stained for NBS1 and either Mre11, Rad50, or E1B55kDa 24 h after infection. The localization of these proteins was visualized by confocal laser microscopy. Scale bar, 100 μm. B, A549 cells were infected with OBP-301 at an MOI of 10 and collected at the indicated time points after infection. Blots were probed with antibodies for Mre11, Rad50, NBS1, and E1B55kDa. C, A549 cells were infected with either Ad-wt, OBP-301, or dl1520 (Onyx-015) at an MOI of 10; stained for Mre11 at 24, 48, and 72 h after infection; and analyzed by confocal laser microscopy. D, the subcellular distribution of Mre11 protein was classified as scattered, perinuclear, and degraded. The proportions of each pattern were determined 24, 48, and 72 h after viral infection. E, quantification of Mre11-positive cells after OBP-301 infection. The relative ratios of cells with scattered staining are plotted against the amount of time since infection.

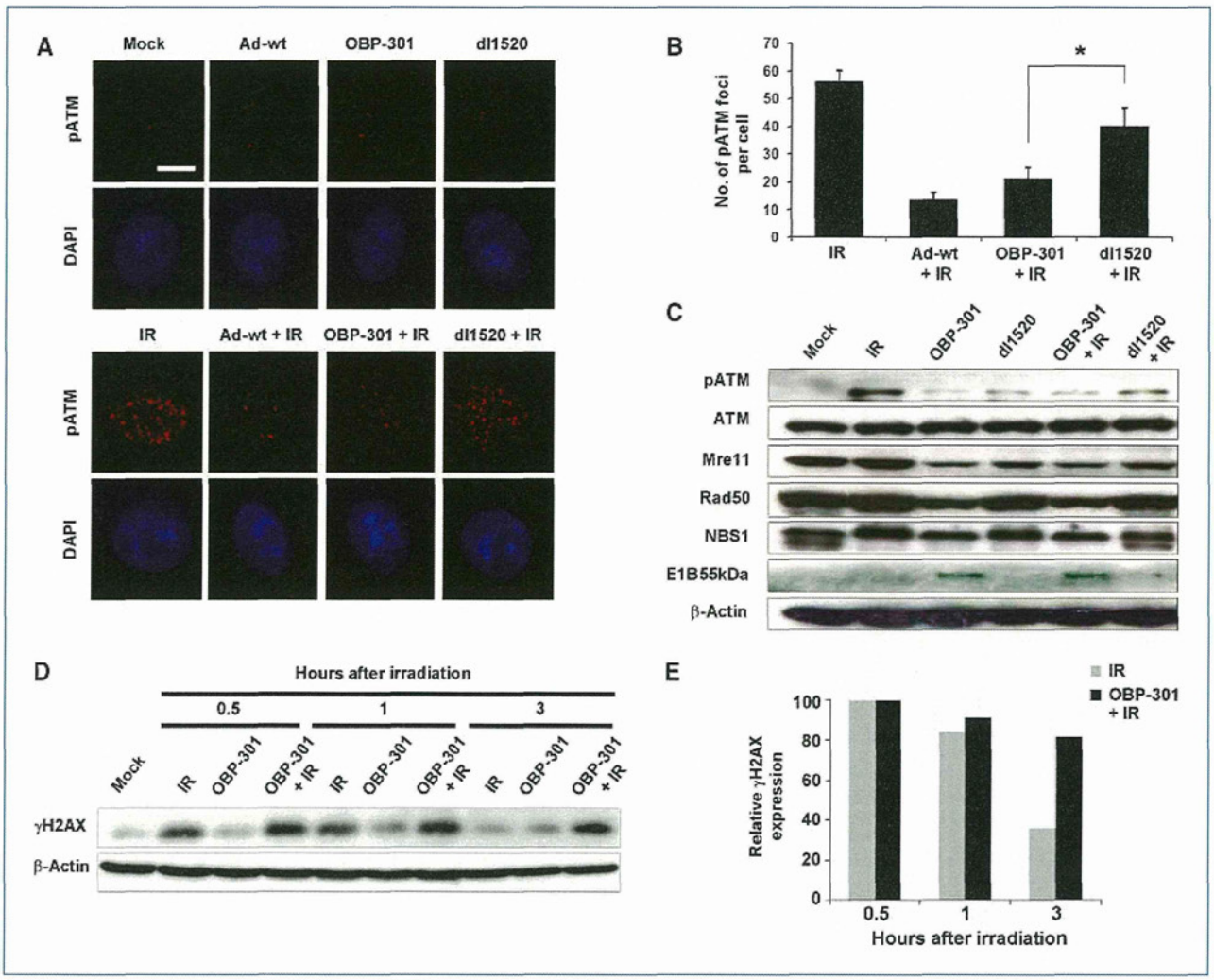

Figure 3. Inhibition of DNA repair by E1B55kDa protein through the blockade of radiation-induced ATM autophosphorylation. A, A549 cells were infected with either Ad-wt, OBP-301, or dl1520 at an MOI of 10 and then irradiated with 10 Gy at 24 h after infection. Nuclear phosphorylated ATM (pATM) foci were visualized 30 min after irradiation by immunofluorescent staining under a confocal laser microscope. Scale bar, 100 μm. B, quantification of pATM foci in treated A549 cells. The numbers of pATM foci per cell were counted in 10 different cells per group. *, $P < 0.01$. C, A549 cells were infected with OBP-301 or dl1520 and irradiated with 10 Gy at 24 h after infection. Cells were then subjected to Western blot analysis for pATM, ATM, Mre11, Rad11, NBS1, E1B55kDa, and β-actin 30 min after irradiation. D, γH2AX expression after irradiation in cells with or without OBP-301 infection. A549 cells were infected with OBP-301 at an MOI of 10 and then irradiated with 10 Gy at 24 h after infection. The cells were harvested at 0.5, 1, and 3 h after irradiation and subjected to Western blot analysis for γH2AX. Note the maintenance of γH2AX in the presence of OBP-301 infection. E, the levels of γH2AX expression were quantified by densitometric scanning with Image J software. The relative γH2AX expression is shown as a percentage of the γH2AX/β-actin value at 30 min after irradiation.

but invariably started to regrow 14 days after the beginning of treatment, whereas OBP-301 plus radiation completely eradicated the established larger TE8 tumors on day 28 in 9 of 10 mice (Fig. 5A).

Tumors treated with OBP-301 or radiation alone were consistently smaller than tumors of the control cohort of mice (Fig. 5B; Supplementary Fig. S8A). Massive ulceration was noted on the tumor surface after injection of OBP-301, whereas no tumor burden was detected when ionizing radiation was combined with OBP-301 injection. Moreover, histologic analysis revealed the apparent destruction of tumor tissues after OBP-301 injection or ionizing radiation. However, no residual tumor cells were observed in tumors treated with OBP-301 plus radiation; instead, massive cellular infiltrates were noted (Supplementary Fig. S8B). Mice with tumor eradication significantly recovered their body weight, although there was a gradual decrease in the body weight of the control group (Supplementary Fig. S9).

Evaluation of *in vivo* antitumor effects on orthotopic human esophageal cancer model

Finally, we assessed the therapeutic efficacy of intratumoral injection of OBP-301 and local irradiation in an orthotopic human esophageal cancer xenograft model by

using noninvasive whole-body imaging. When TE8 human esophageal cancer cells stably transfected with the luciferase gene (TE8-Luc) were s.c. implanted into nude mice, a correlation was observed between tumor growth (volume) and the luciferase emission level (luminescent intensity; Supplementary Fig. S10). Our preliminary experiments revealed that when TE8-Luc cells were inoculated into the wall of the abdominal esophagus of athymic *nu/nu* mice, esophageal tumors appeared within 3 weeks after tumor injection (Fig. 5C).

Mice bearing macroscopic esophageal tumors were treated with local irradiation at 2 Gy followed by intratumoral injection during laparotomy of 1×10^8 PFU of OBP-301 every 2 days for three cycles. The luminescent intensity of tumors treated with OBP-301 plus radiation was significantly lower than that of mock-treated, irradiated, or OBP-301–injected tumors (Fig. 5D and E). These results suggest that the biochemical interaction of OBP-301 with irradiation can be translated into a potential clinically applicable cancer treatment.

Discussion

A novel biological property of OBP-301 as a molecular radiosensitizer was verified, referring to a critical role of adenoviral E1B55kDa in inhibiting the DNA damage responses triggered by ionizing radiation. Radiation-induced cell death is dependent on DNA damage and, therefore, inhibition of

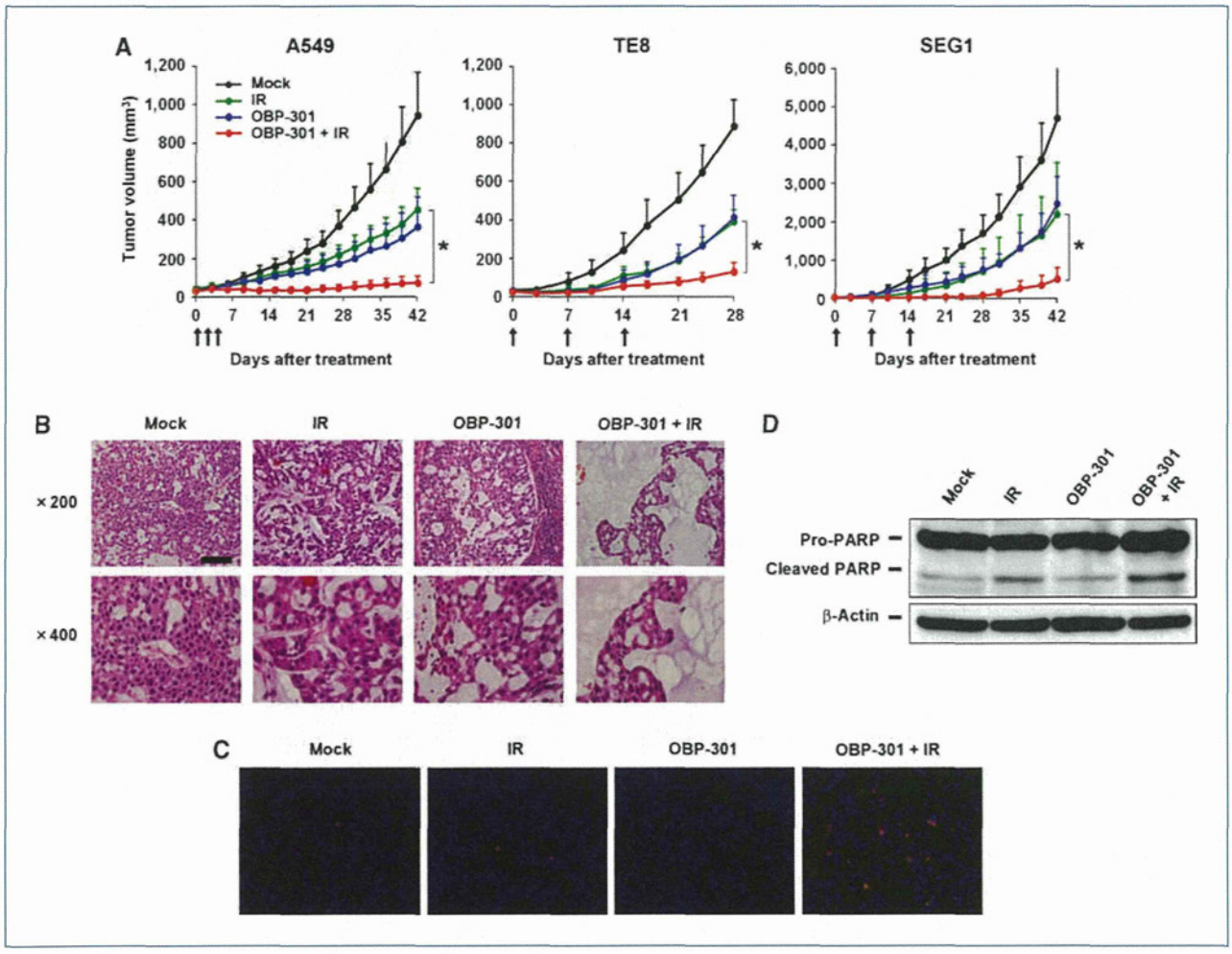

Figure 4. Antitumor effects of OBP-301 and ionizing radiation against s.c. established xenograft tumors. A, cells (2×10^6 per mouse) were injected s.c. into the right flanks of mice. When the tumors reached 3 to 5 mm in diameter, mice were exposed to 3 Gy (for A549) or 2 Gy (for TE8 and SEG1) of ionizing radiation and intratumorally administered OBP-301 (1×10^8 PFU/tumor) for three cycles every 2 d (for A549) or every week (for TE8 and SEG1). Six (for A549) or eight (for TE8 and SEG1) mice were used for each group. Tumor growth is expressed as the mean tumor volume ± SD. Arrows indicate each treatment. *, $P < 0.01$. B, mice bearing A549 xenografts were treated as described above. Tumor sections were obtained 10 d after the final administration of OBP-301. Paraffin sections of tumors were stained with hematoxylin and eosin. Scale bar, 100 μm. Magnification, ×200 (top), ×400 (bottom). C and D, *in vivo* induction of apoptotic cell death by OBP-301 and ionizing radiation. C, paraffin-embedded sections of A549 subcutaneous tumors excised 3 d after treatment as described above were subjected to TUNEL staining. D, Western blot analysis for PARP and β-actin was done with proteins extracted from A549 subcutaneous tumors 3 d after treatments.

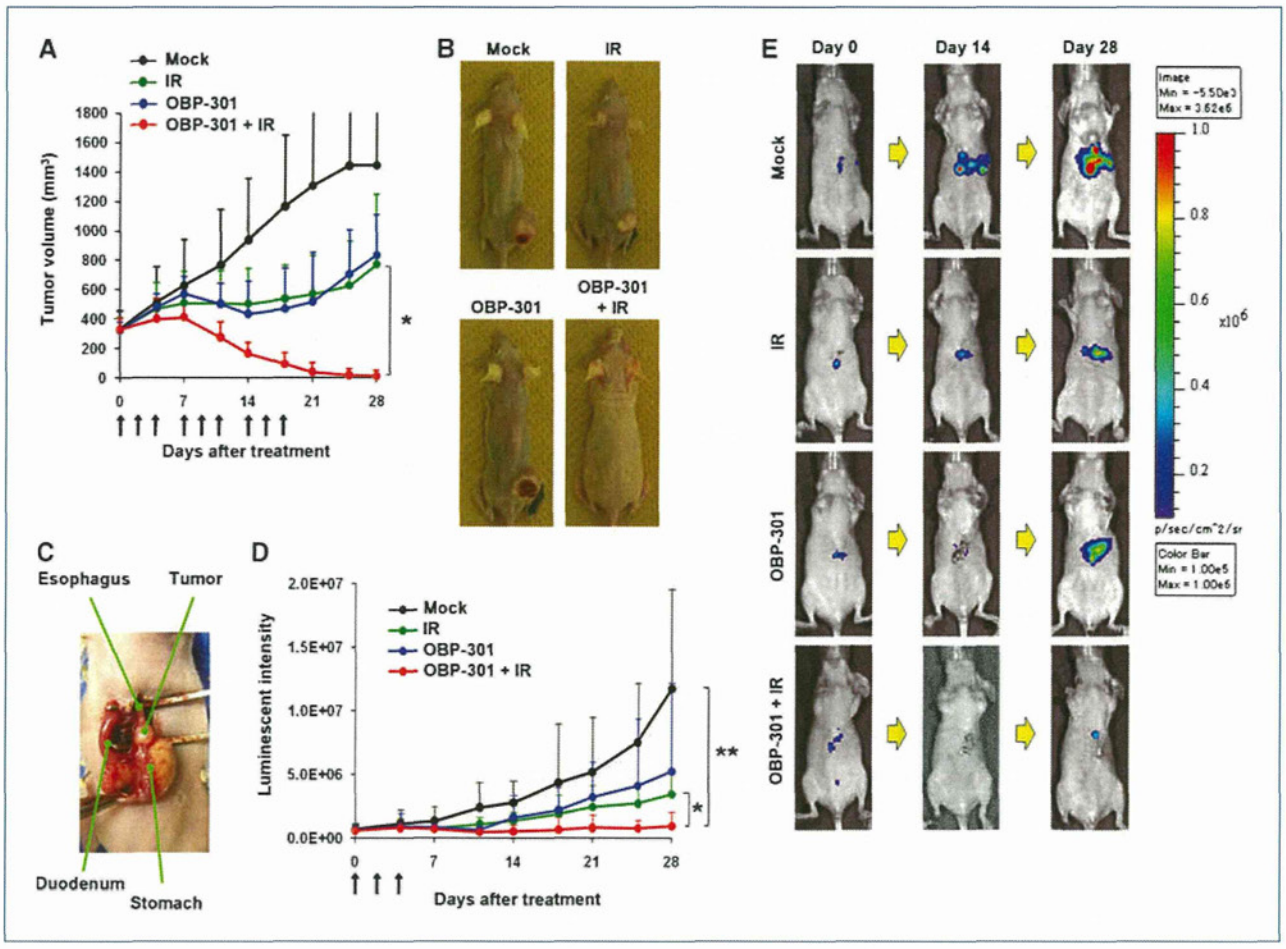

Figure 5. *In vivo* antitumor effects of OBP-301 and ionizing radiation against TE8 human esophageal cancer xenografts. A, larger subcutaneous TE8 tumors with a diameter of 8 to 10 mm were treated with OBP-301 followed by ionizing radiation three times per week (every 2 d) for three cycles (nine times in total). Ten mice were used for each group. Tumor growth is expressed as mean tumor volume ± SD. Arrows indicate each treatment. *, $P < 0.01$. B, macroscopic appearance of representative tumors 28 d after treatment. C, macroscopic appearance of orthotopic TE8-Luc esophageal tumor 3 wk after tumor cell inoculation (2×10^6 cells per mouse). D, mice bearing orthotopic TE8-Luc tumors were exposed to 2 Gy of ionizing radiation and intratumorally administered OBP-301 (1×10^8 PFU/tumor) for three cycles every 2 d. The luminescent intensity was measured by the IVIS imaging system 10 to 30 min after peritoneal administration of luciferin. Tumor growth is expressed by the luminescent intensity ± SD. Arrows indicate each treatment. *, $P < 0.01$; **, $P < 0.05$. E, representative images of mice treated with either ionizing radiation, OBP-301, or both on days 0, 14, and 28.

DNA repair can enhance the sensitivity of human tumor cells to ionizing radiation. The ATM activation by the MRN complex is essential for sensing and signaling from DNA DSBs and plays an important role in DNA repair and checkpoints, indicating that this pathway may be a good target for enhancing the antitumor effects of DNA-damaging agents. Indeed, ATM inhibitors, such as KU55933 and CGK733, and an MRN complex inhibitor, mirin, could sensitize cancer cells to therapeutic agents that cause DNA DSBs (21–23). Hsp90 interacts with the MRN complex, and an Hsp90 inhibitor enhances the sensitivity of tumor cells to radiation (24). Molecular disruption of MRN function by a dominant-negative mutant *Rad50* gene transfer sensitizes tumor cells to cisplatin (25). Although these approaches are effective in interrupting cellular DNA repair mechanisms, they lack tumor selectivity and may damage normal tissues when combined with DNA-damaging therapies. Our data show that OBP-301 could synergize with ionizing radiation only in tumor cells but not in normal cells due to its telomerase dependency, suggesting that the regional administration of OBP-301 enables targeted radiosensitization.

The adenovirus *E1B* gene encodes a 19-kDa polypeptide (*E1B19kDa*) and a 55-kDa protein (*E1B55kDa*). The E1B55kDa protein induces a cellular environment conducive for viral protein synthesis via a complex with the E4orf6 protein (26). This E1B55kDa/E4orf6 complex degrades the MRN complex, blocks the downstream ATM signaling, and leads to a defective G_2-M checkpoint in response to DSBs (10). Although the impact of E1B55kDa-mediated disruption of the MRN-ATM pathway on the DNA damage responses triggered by ionizing radiation has not yet been studied, we showed that OBP-301–mediated E1B55kDa expression induced the degradation of all components of the MRN

complex, which in turn prevented ATM autophosphorylation following ionizing radiation. OBP-301 expresses the *E1B* gene under the control of the hTERT promoter through an internal ribosome entry site sequence, whereas dl1520 (Onyx-015, CI-1042), which has been used in many clinical trials, was genetically modified by disruption of the coding sequence of the E1B55kDa protein (19). Therefore, ionizing radiation–induced ATM activation was blocked more efficiently by OBP-301 than by dl1520, which lacks E1B55kDa, although dl1520 slightly inhibited ATM phosphorylation, presumably due to E4orf6 protein expression (27).

One hallmark of DNA DSBs is the phosphorylation of H2AX at Ser139, a specialized histone H2A variant (referred to as γH2AX; ref. 28); the reduction in γH2AX levels in irradiated cells correlates with the repair of DSBs (29). OBP-301 infection apparently sustained the elevated levels of γH2AX longer in irradiated tumor cells, indicating that tumor cells infected with OBP-301 could be rendered sensitive to ionizing radiation. We previously found that the process of oncolysis is morphologically distinct from apoptosis and necrosis, although autophagy is partially involved in this effect (30). The observation that OBP-301 infection significantly enhanced the induction of apoptosis when combined with ionizing radiation suggests that the radiosensitizing activity of OBP-301 is independent of virus-mediated oncolysis. Indeed, dephosphorylation of H2AX is associated with efficient DNA repair, whereas a pronounced increase in H2AX phosphorylation correlates with apoptosis (31, 32). Moreover, synergistically enhanced apoptosis by OBP-310 and ionizing radiation is likely to be p53 independent because p53 was ubiquitinated and degraded by E1B55kDa and E4orf6 proteins (16, 18).

Our *in vitro* studies suggest that OBP-301 infection and ionizing radiation may mutually sensitize human tumor cells, potentially leading to an effective combination treatment. OBP-301 infection requires a period of replication to induce the cytopathic effect and to sensitize cells to radiation, whereas ionizing radiation immediately causes DNA DSBs. Therefore, in a true clinical setting, multiple cycles of the external-beam radiotherapy followed by intratumoral injection of OBP-301 may yield optimal results. We confirmed the synergistic antitumor effect of three cycles of treatment with OBP-301 plus regional radiation and the *in vivo* induction of apoptotic cell death on subcutaneous human tumor xenografts. The orthotopic implantation of tumor cells, however, restores the correct tumor-host interactions, which do not occur when tumors are implanted in ectopic subcutaneous sites (33). Thus, we also showed the significant synergy of combined treatments in an orthotopic mouse model of human esophageal cancer by using a noninvasive whole-body imaging system.

There are some possible advantages of combining virotherapy with radiotherapy *in vivo*. First, OBP-301 may inhibit the vascular supply by killing endothelial cells because endothelial cell proliferation is increased in irradiated tumors (34), presumably with high telomerase activity. Alternatively, local irradiation itself may attack the vascular endothelial cells in the tumor site, which in turn can block the escape of locally injected OBP-301 into the blood circulation. Indeed, ionizing radiation inhibits endothelial cell proliferation, tube formation, migration, and clonogenic survival (35). Furthermore, in an immunocompetent environment, as we previously reported (36), OBP-301 stimulates host immune cells to produce endogenous antiangiogenic factors such as interferon-γ. Second, virotherapy and radiotherapy may target tumor cells in different parts of tumors with distinct mechanisms. For example, tumor hypoxia has been considered a potential therapeutic problem because it renders tumor cells more resistant to ionizing radiation (37) and, therefore, some cells in certain parts of tumors may survive and proliferate under hypoxic conditions. In contrast, because hypoxia induces the transcriptional activity of hTERT gene promoter through hypoxia-inducible factor 1α (38), OBP-301 can be expected to replicate and efficiently kill tumor cells even under hypoxic conditions. Thus, hTERT-specific oncolytic virotherapy can be effective in eliminating tumor cells that survive after local radiotherapy.

Another advantage of this combination therapy is that the area where each treatment shows the therapeutic effect is overlapping. The treatment field of radiotherapy includes primary tumors and regional lymph nodes. We previously showed that intratumorally injected OBP-301 expressing the *GFP* gene is effectively transported into the lymphatic circulation; viral replication produced GFP fluorescence signals in the metastatic lymph nodes in orthotopic human colorectal and oral cancer xenograft models (39, 40). Therefore, we anticipate that intratumoral OBP-301 administration will radiosensitize both primary tumors and regional lymph nodes.

In summary, our data show the molecular basis of radiosensitization induced by telomerase-specific virotherapy, in which the adenoviral E1B55kDa protein inhibits the radiation-induced DNA repair machinery through the interruption of the MRN function. OBP-301 infection and ionizing radiation mutually modulate their respective biological effects and thereby potentiate each other, profoundly enhancing *in vivo* antitumor activity in an orthotopic mouse model.

Disclosure of Potential Conflicts of Interest

Y. Urata is an employee of Oncolys BioPharma, Inc., the manufacturer of OBP-301 (Telomelysin). The other authors disclosed no potential conflicts of interest.

Acknowledgments

We thank Dr. Frank McCormick (University of California at San Francisco Helen Diller Family Comprehensive Cancer Center) for supplying the E1B55kDa-defective adenovirus mutant dl1520 (Onyx-015), and Tomoko Sueishi and Mitsuko Yokota for their excellent technical support.

Grant Support

Ministry of Education, Culture, Sports, Science, and Technology of Japan (Toshiyoshi Fujiwara) and Ministry of Health, Labour, and Welfare of Japan (Toshiyoshi Fujiwara).

The costs of publication of this article were defrayed in part by the payment of page charges. This article must therefore be hereby marked *advertisement* in accordance with 18 U.S.C. Section 1734 solely to indicate this fact.

Received 06/29/2010; revised 09/13/2010; accepted 09/17/2010; published OnlineFirst 11/02/2010.

References

1. Bentzen SM, Harari PM, Bernier J. Exploitable mechanisms for combining drugs with radiation: concepts, achievements and future directions. Nat Clin Pract Oncol 2007;4:172–80.
2. Bradley KA, Pollack IF, Reid JM, et al. Motexafin gadolinium and involved field radiation therapy for intrinsic pontine glioma of childhood: a Children's Oncology Group phase I study. Neuro Oncol 2008;10:752–8.
3. Hoskin P, Rojas A, Saunders M. Accelerated radiotherapy, carbogen, and nicotinamide (ARCON) in the treatment of advanced bladder cancer: mature results of a Phase II nonrandomized study. Int J Radiat Oncol Biol Phys 2009;73:1425–31.
4. Kim CH, Park SJ, Lee SH. A targeted inhibition of DNA-dependent protein kinase sensitizes breast cancer cells following ionizing radiation. J Pharmacol Exp Ther 2002;303:753–9.
5. Tang X, Hui ZG, Cui XL, Garg R, Kastan MB, Xu B. A novel ATM-dependent pathway regulates protein phosphatase 1 in response to DNA damage. Mol Cell Biol 2008;28:2559–66.
6. Shiloh Y. Ataxia-telangiectasia and the Nijmegen breakage syndrome: related disorders but genes apart. Annu Rev Genet 1997; 31:635–62.
7. Petrini JH. The Mre11 complex and ATM: collaborating to navigate S phase. Curr Opin Cell Biol 2000;12:293–6.
8. Sturgeon CM, Roberge M. G2 checkpoint kinase inhibitors exert their radiosensitizing effects prior to the G2/M transition. Cell Cycle 2007; 6:572–5.
9. D'Amours D, Jackson SP. The Mre11 complex: at the crossroads of DNA repair and checkpoint signalling. Nat Rev Mol Cell Biol 2002;3: 317–27.
10. Carson CT, Schwartz RA, Stracker TH, Lilley CE, Lee DV, Weitzman MD. The Mre11 complex is required for ATM activation and the G2/M checkpoint. EMBO J 2003;22:6610–20.
11. Theunissen JW, Kaplan MI, Hunt PA, et al. Checkpoint failure and chromosomal instability without lymphomagenesis in Mre11 (ATLD1/ATLD1) mice. Mol Cell 2003;12:1511–23.
12. Kawashima T, Kagawa S, Kobayashi N, et al. Telomerase-specific replication-selective virotherapy for human cancer. Clin Cancer Res 2004;10:285–92.
13. Umeoka T, Kawashima T, Kagawa S, et al. Visualization of intrathoracically disseminated solid tumors in mice with optical imaging by telomerase-specific amplification of a transferred green fluorescent protein gene. Cancer Res 2004;64:6259–65.
14. Taki M, Kagawa S, Nishizaki M, et al. Enhanced oncolysis by a tropism-modified telomerase-specific replication-selective adenoviral agent OBP-405 ('Telomelysin-RGD'). Oncogene 2005;24:3130–40.
15. Hashimoto Y, Watanabe Y, Shirakiya Y, et al. Establishment of biological and pharmacokinetic assays of telomerase-specific replication-selective adenovirus. Cancer Sci 2008;99:385–90.
16. Querido E, Marcellus RC, Lai A, et al. Regulation of p53 levels by the E1B 55-kilodalton protein and E4orf6 in adenovirus-infected cells. J Virol 1997;71:3788–98.
17. Stracker TH, Carson CT, Weitzman MD. Adenovirus oncoproteins inactivate the Mre11-50-NBS1 DNA repair complex. Nature 2002;418: 348–52.
18. Schwartz RA, Lakdawala SS, Eshleman HD, Russell MR, Carson CT, Weitzman MD. Distinct requirements of adenovirus E1b55K protein for degradation of cellular substrates. J Virol 2008;82:9043–55.
19. Bischoff JR, Kirn DH, Williams A, et al. An adenovirus mutant that replicates selectively in p53-deficient human tumor cells. Science 1996;274:373–6.
20. Chou TC. Theoretical basis, experimental design, and computerized simulation of synergism and antagonism in drug combination studies. Pharmacol Rev 2006;58:621–81.
21. Crescenzi E, Palumbo G, de BJ, Brady HJ. Ataxia telangiectasia mutated and p21CIP1 modulate cell survival of drug-induced senescent tumor cells: implications for chemotherapy. Clin Cancer Res 2008; 14:1877–87.
22. Cheng WH, Muftic D, Muftuoglu M, et al. WRN is required for ATM activation and the S-phase checkpoint in response to interstrand cross-link-induced DNA double-strand breaks. Mol Biol Cell 2008; 19:3923–33.
23. Dupre A, Boyer-Chatenet L, Sattler RM, et al. A forward chemical genetic screen reveals an inhibitor of the Mre11-50-Nbs1 complex. Nat Chem Biol 2008;4:119–25.
24. Dote H, Burgan WE, Camphausen K, Tofilon PJ. Inhibition of hsp90 compromises the DNA damage response to radiation. Cancer Res 2006;66:9211–20.
25. Abuzeid WM, Jiang X, Shi G, et al. Molecular disruption of RAD50 sensitizes human tumor cells to cisplatin-based chemotherapy. J Clin Invest 2009;119:1974–85.
26. Blackford AN, Grand RJ. Adenovirus E1B 55-kilodalton protein: multiple roles in viral infection and cell transformation. J Virol 2009;83: 4000–12.
27. Hart LS, Yannone SM, Naczki C, et al. The adenovirus E4orf6 protein inhibits DNA double strand break repair and radiosensitizes human tumor cells in an E1B-55K-independent manner. J Biol Chem 2005; 280:1474–81.
28. Redon C, Pilch D, Rogakou E, Sedelnikova O, Newrock K, Bonner W. Histone H2A variants H2AX and H2AZ. Curr Opin Genet Dev 2002; 12:162–9.
29. Banath JP, Macphail SH, Olive PL. Radiation sensitivity, H2AX phosphorylation, and kinetics of repair of DNA strand breaks in irradiated cervical cancer cell lines. Cancer Res 2004;64:7144–9.
30. Endo Y, Sakai R, Ouchi M, et al. Virus-mediated oncolysis induces danger signal and stimulates cytotoxic T-lymphocyte activity via proteasome activator upregulation. Oncogene 2008;27:2375–81.
31. Ewald B, Sampath D, Plunkett W. H2AX phosphorylation marks gemcitabine-induced stalled replication forks and their collapse upon S-phase checkpoint abrogation. Mol Cancer Ther 2007;6:1239–48.
32. Cook PJ, Ju BG, Telese F, Wang X, Glass CK, Rosenfeld MG. Tyrosine dephosphorylation of H2AX modulates apoptosis and survival decisions. Nature 2009;458:591–6.
33. Fidler IJ. Rationale and methods for the use of nude mice to study the biology and therapy of human cancer metastasis. Cancer Metastasis Rev 1986;5:29–49.
34. Tsai JH, Makonnen S, Feldman M, Sehgal CM, Maity A, Lee WM. Ionizing radiation inhibits tumor neovascularization by inducing ineffective angiogenesis. Cancer Biol Ther 2005;4:1395–400.
35. Abdollahi A, Lipson KE, Sckell A, et al. Combined therapy with direct and indirect angiogenesis inhibition results in enhanced antiangiogenic and antitumor effects. Cancer Res 2003;63:8890–8.
36. Ikeda Y, Kojima T, Kuroda S, et al. A novel antiangiogenic effect for telomerase-specific virotherapy through host immune system. J Immunol 2009;182:1763–9.
37. Hockel M, Vaupel P. Tumor hypoxia: definitions and current clinical, biologic, and molecular aspects. J Natl Cancer Inst 2001;93:266–76.
38. Nishi H, Nakada T, Kyo S, Inoue M, Shay JW, Isaka K. Hypoxia-inducible factor 1 mediates upregulation of telomerase (hTERT). Mol Cell Biol 2004;24:6076–83.
39. Kishimoto H, Kojima T, Watanabe Y, et al. *In vivo* imaging of lymph node metastasis with telomerase-specific replication-selective adenovirus. Nat Med 2006;12:1213–9.
40. Kurihara Y, Watanabe Y, Onimatsu H, et al. Telomerase-specific virotheranostics for human head and neck cancer. Clin Cancer Res 2009;15:2335–43.

Published OnlineFirst February 16, 2011; DOI:10.1158/1078-0432.CCR-10-2066

Cancer Therapy: Preclinical

Clinical Cancer Research

Preclinical Evaluation of Telomerase-Specific Oncolytic Virotherapy for Human Bone and Soft Tissue Sarcomas

Tsuyoshi Sasaki[1], Hiroshi Tazawa[2,3], Jo Hasei[1], Toshiyuki Kunisada[1,4], Aki Yoshida[1], Yuuri Hashimoto[3], Shuya Yano[3], Ryosuke Yoshida[3], Futoshi Uno[2,3], Shunsuke Kagawa[2,3], Yuki Morimoto[1], Yasuo Urata[5], Toshifumi Ozaki[1], and Toshiyoshi Fujiwara[2,3]

Abstract

Purpose: Tumor-specific replication-selective oncolytic virotherapy is a promising antitumor therapy for induction of cell death in tumor cells but not of normal cells. We previously developed an oncolytic adenovirus, OBP-301, that kills human epithelial malignant cells in a telomerase-dependent manner. Recent evidence suggests that nonepithelial malignant cells, which have low telomerase activity, maintain telomere length through alternative lengthening of telomeres (ALT). However, it remains unclear whether OBP-301 is cytopathic for nonepithelial malignant cells. Here, we evaluated the antitumor effect of OBP-301 on human bone and soft tissue sarcoma cells.

Experimental Design: The cytopathic activity of OBP-301, coxsackie and adenovirus receptor (CAR) expression, and telomerase activity were examined in 10 bone (OST, U2OS, HOS, HuO9, MNNG/HOS, SaOS-2, NOS-2, NOS-10, NDCS-1, and OUMS-27) and in 4 soft tissue (CCS, NMS-2, SYO-1, and NMFH-1) sarcoma cell lines. OBP-301 antitumor effects were assessed using orthotopic tumor xenograft models. The fiber-modified OBP-301 (termed OBP-405) was used to confirm an antitumor effect on OBP-301–resistant sarcomas.

Results: OBP-301 was cytopathic for 12 sarcoma cell lines but not for the non–CAR-expressing OUMS-27 and NMFH-1 cells. Sensitivity to OBP-301 was dependent on CAR expression and not on telomerase activity. ALT-type sarcomas were also sensitive to OBP-301 because of upregulation of human telomerase reverse transcriptase (*hTERT*) mRNA following virus infection. Intratumoral injection of OBP-301 significantly suppressed the growth of OST and SYO-1 tumors. Furthermore, fiber-modified OBP-405 showed antitumor effects on OBP-301–resistant OUMS-27 and NMFH-1 cells.

Conclusions: A telomerase-specific oncolytic adenovirus is a promising antitumor reagent for the treatment of bone and soft tissue sarcomas. *Clin Cancer Res; 17(7); 1828–38. ©2011 AACR.*

Introduction

Bone and soft tissue sarcomas are annually diagnosed in 13,230 patients in the United States (1). They are the third most common cancer in children and account for 15.4% of all childhood malignancies. Treatment of patients with bone and soft tissue sarcomas requires a multidisciplinary approach that involves orthopedic oncologists, musculoskeletal radiologists and pathologists, radiation oncologists, medical and pediatric oncologists, and microvascular surgeons (2, 3). Despite major advances in the treatment of bone and soft tissue sarcomas, such as neoadjuvant and adjuvant multiagent chemotherapy and aggressive surgery, about one fourth of the patients show a poor response to conventional therapy, resulting in subsequent recurrence and leading to a poor prognosis (1). Therefore, the development of a novel therapeutic strategy is required to cure patients with bone and soft tissue sarcomas.

Recent advances in molecular biology have fostered remarkable insights into the molecular basis of neoplasia. More than 85% of all human cancers, but only a few normal somatic cells, show high telomerase activity (4–6). Telomerase activity has also been detected in 17% to 81% of bone and soft tissue sarcomas (7–10). Telomerase activation is considered to be a critical step in cancer development, and its activity is closely correlated with the expression of human telomerase reverse transcriptase

Authors' Affiliations: [1]Department of Orthopaedic Surgery, Okayama University Graduate School of Medicine, Dentistry and Pharmaceutical Sciences; [2]Center for Gene and Cell Therapy, Okayama University Hospital; Departments of [3]Gastroenterological Surgery and [4]Medical Materials for Musculoskeletal Reconstruction, Okayama University Graduate School of Medicine, Dentistry and Pharmaceutical Sciences, Okayama; and [5]Oncolys BioPharma, Inc., Tokyo, Japan

Note: Supplementary data for this article are available at Clinical Cancer Research Online (http://clincancerres.aacrjournals.org/).

Corresponding Author: Toshiyoshi Fujiwara, Department of Gastroenterological Surgery, Okayama University Graduate School of Medicine, Dentistry and Pharmaceutical Sciences, 2-5-1 Shikata-cho, Kita-ku, Okayama 700-8558, Japan. Phone: 81-86-235-7257; Fax: 81-86-221-8775. E-mail: toshi_f@md.okayama-u.ac.jp

doi: 10.1158/1078-0432.CCR-10-2066

Published OnlineFirst February 16, 2011; DOI:10.1158/1078-0432.CCR-10-2066

Translational Relevance

Bone and soft tissue sarcomas frequently occur in young children and show aggressive progression, resistance to conventional chemotherapy, and poor prognosis, indicating a requirement for novel antitumor therapy to improve the clinical outcome. Telomerase-specific replication-selective oncolytic virotherapy is emerging as a promising antitumor therapy. We developed an oncolytic adenovirus, OBP-301, that efficiently kills human epithelial malignant cells in a telomerase-dependent manner. However, alternative lengthening of telomeres (ALT)-type nonepithelial malignant cells show low telomerase activity, suggesting lower effectiveness of OBP-301 in these cells. Here, we showed that OBP-301 has antitumor effects on both non–ALT-type and ALT-type sarcoma cells through upregulation of human telomerase reverse transcriptase mRNA. Furthermore, coxsackie and adenovirus receptor–negative sarcoma cells were efficiently killed by fiber-modified OBP-301 (termed OBP-405) through virus–integrin binding. Thus, a telomerase-specific oncolytic adenovirus would greatly improve the clinical outcome of young patients with advanced sarcomas.

(*hTERT*; ref. 11). Recently, telomerase-specific replication-selective oncolytic virotherapy has emerged as a promising antitumor therapy for induction of tumor-specific cell death. We previously developed an oncolytic adenovirus, OBP-301, in which the *hTERT* promoter drives the expression of the *E1A* and *E1B* genes linked to an internal ribosome entry site (IRES; ref. 12). We determined that OBP-301 efficiently induced the selective killing of a variety of human malignant epithelial cells, such as colorectal, prostate, and non–small cell lung cancers, but not of normal cells (12, 13). Furthermore, a phase I clinical trial of OBP-301, which was conducted in the United States on patients with advanced solid tumors, indicated that OBP-301 is well tolerated by patients (14).

There are 2 known telomere-maintenance mechanisms in human malignant tumors (15, 16): telomerase activation (4–6) and telomerase-independent alternative lengthening of telomeres (ALT; ref. 17–19). The ALT-type mechanism is more prevalent in tumors arising from nonepithelial tissues than in those of epithelial origin (20, 21). Therefore, ALT-type nonepithelial malignant cells frequently show low telomerase activity, suggesting that they have a low sensitivity to OBP-301, which kills cancer cells in a telomerase-dependent manner. However, it remains to be determined whether OBP-301 can exert an antitumor effect on human nonepithelial and on epithelial malignancies.

Adenovirus infection is mainly mediated by interaction of the virus with the coxsackie and adenovirus receptor (CAR) expressed on host cells (22). Therefore, while CAR-expressing tumor cells are the main targets for oncolytic adenoviruses, tumor cells that lack CAR can escape from being killed by oncolytic adenoviruses. It has been reported that CAR is frequently expressed in human cancers of various organs such as the brain (23), thyroid (24), esophagus (25), gastrointestinal tract (26), and ovary (27). Bone and soft tissue sarcomas also express CAR (28–30). However, some populations of tumor cells lack CAR expression, suggesting a requirement for the development of a novel antitumor therapy against CAR-negative tumor cells. We recently developed fiber-modified OBP-301 (termed OBP-405), which can bind to not only CAR but also integrin molecules ($\alpha v\beta 3$ and $\alpha v\beta 5$) and efficiently kill CAR-negative tumor cells (31).

In the present study, we first investigated the *in vitro* cytopathic efficacy of OBP-301 against 14 human bone and soft tissue sarcoma cells. Next, the relationship between the cytopathic activity of OBP-301, CAR expression, and telomerase activity in human sarcoma cells was assessed. The *in vivo* antitumor effect of OBP-301 was also confirmed using orthotopic animal models. Finally, the antitumor effect of OBP-405 against OBP-301–resistant sarcoma cells was evaluated *in vitro* and *in vivo*.

Materials and Methods

Cell lines

The human osteosarcoma (HuO9; ref. 32), chondrosarcoma (OUMS-27; ref. 33), and synovial sarcoma (SYO-1; ref. 34) cell lines were previously established in our laboratory. The human osteosarcoma cell lines OST, HOS, and SaOS-2 were kindly provided by Dr. Satoru Kyo (Kanazawa University, Ishikawa, Japan). The human clear cell sarcoma cell line CCS was maintained in our laboratory. These cells were propagated as monolayer cultures in Dulbecco's modified Eagle's medium (DMEM). The human osteosarcoma cell line U2OS was obtained from the American Type Culture Collection (ATCC) and was grown in McCoy's 5a medium. The human osteosarcoma cell line MNNG/HOS was purchased from DS Pharma Biomedical and was maintained in Eagle's minimum essential medium containing 1% nonessential amino acids. The human osteosarcoma cell lines NOS-2 and NOS-10 (35), the human dedifferentiated chondrosarcoma cell line NDCS-1 (36), the human malignant peripheral nerve sheath cell line NMS-2 (37), and the human malignant fibrous histiocytoma cell line NMFH-1 (38) were kindly provided by Dr. Hiroyuki Kawashima (Niigata University, Niigata, Japan) and were grown in RPMI-1640 medium. The transformed embryonic kidney cell line 293 was obtained from the ATCC and maintained in DMEM. All media were supplemented with 10% heat-inactivated FBS, 100 units/mL penicillin, and 100 μg/mL streptomycin. The cells were maintained at 37°C in a humidified atmosphere with 5% CO_2.

Recombinant adenoviruses

The recombinant tumor-specific, replication-selective adenovirus OBP-301 (Telomelysin), in which the promoter

Published OnlineFirst February 16, 2011; DOI:10.1158/1078-0432.CCR-10-2066

element of the *hTERT* gene drives the expression of *E1A* and *E1B* genes linked with an IRES, was previously constructed and characterized (12, 13). OBP-405 is a telomerase-specific replication-competent adenovirus variant that was previously generated to express the RGD peptide in the fiber knob of OBP-301 (31). The *E1A*-deleted adenovirus vector dl312 and wild-type adenovirus serotype 5 (Ad5) were used as the control vectors. Recombinant viruses were purified by ultracentrifugation using cesium chloride step gradients, and their titers were determined by a plaque-forming assay by using 293 cells and they were stored at −80°C.

Cell viability assay

Cells were seeded on 96-well plates at a density of 1×10^3 cells/well 20 hours before viral infection. All cell lines were infected with OBP-301 or OBP-405 at multiplicity of infections (MOI) of 0, 0.1, 1, 10, 50, or 100 plaque forming units (PFU)/cell. Cell viability was determined on days 1, 2, 3, and 5 after virus infection, using a Cell Proliferation kit II (Roche Molecular Biochemicals) that was based on an XTT, sodium 3′-[1-(phenylaminocarbonyl)-3,4-tetrazolium]-bis (4-methoxy-6-nitro)benzene sulfonic acid hydrate, assay, according to the manufacturer's protocol. The ID_{50} value of OBP-301 for each cell line was calculated using cell viability data obtained on day 5 after virus infection.

Flow cytometric analysis

The cells (5×10^5) were labeled with mouse monoclonal anti-CAR (RmcB; Upstate Biotechnology), anti-human integrin αvβ3 (LM609; Chemicon International), or anti-human integrin αvβ5 (P1F6; Chemicon International) antibody for 30 minutes at 4°C. The cells were then incubated with fluorescein isothiocyanate (FITC)-conjugated rabbit anti-mouse IgG second antibody (Zymed Laboratories) and were analyzed using flow cytometry (FACS Array; Becton Dickinson). The mean fluorescence intensity (MFI) of CAR and integrin αvβ3 or αvβ5 for each cell line was determined by calculating the difference between the MFI in antibody-treated and nontreated cells from 3 independent experiments.

Quantitative real-time PCR analysis

U2OS cells, seeded on 6-well plates at a density of 5×10^5 cells/well 20 hours before viral infection, were infected with Ad5, OBP-301, or dl312 at an MOI of 10 or 100 PFUs/cell. Mock-infected cells were used as controls. Furthermore, to confirm the modulation of *hTERT* mRNA expression by OBP-301 infection, CAR-positive and *hTERT* mRNA-expressing human sarcoma cell lines were seeded on 6-well plates at a density of 5×10^4 cells/well 20 hours before viral infection and were infected with OBP-301 at an MOI of 100 PFUs/cell. Total RNA was extracted from the cells 2 days after virus infection by using the RNA-Bee reagent (Tel-Test Inc.). After synthesis of cDNA from 100 ng of total RNA, the levels of *hTERT* and glyceraldehyde-3-phosphate dehydrogenase (*GAPDH*) mRNA expression were determined using quantitative real-time PCR and a Step One Plus Real Time PCR System (Applied Biosystems) and TaqMan Gene Expression Assays (Applied Biosystems). The relative levels of *hTERT* mRNA expression were calculated by using the $2^{-\Delta\Delta Ct}$ method (39) after normalization with reference to the expression of *GAPDH* mRNA.

To compare the *E1A* copy number between OBP-301- and Ad5-infected U2OS cells, U2OS cells, seeded on 6-well plates at a density of 5×10^5 cells/well 20 hours before viral infection, were infected with OBP-301 or Ad5 at an MOI of 10 PFUs/cell. Genomic DNA was extracted from serially diluted viral stocks, and tumor cells were infected with OBP-301 or Ad5 by using the QIAmp DNA Mini Kit (Qiagen). *E1A* copy number was also determined using TaqMan real-time PCR systems (Applied Biosystems).

In vivo OST and OUMS-27 xenograft tumor models

Animal experimental protocols were approved by the Ethics Review Committee for Animal Experimentation of Okayama University School of Medicine. The OST and OUMS-27 cells (5×10^6 cells per site) were inoculated into the tibia or the flank of female athymic nude mice aged 6 to 7 weeks (Charles River Laboratories). Palpable tumors developed within 14 to 21 days and were permitted to grow to approximately 5 to 6 mm in diameter. At that stage, a 50 μL volume of solution containing OBP-301, OBP-405, dl312, or PBS was injected into the tumors. Tumor size was monitored by measuring tumor length and width by using calipers. The volumes of OUMS-27 tumors were calculated using the following formula: $(L \times W^2) \times 0.5$, where L is the length and W is the width of each tumor. The volumes of OST tumors were calculated using the formula: $(L + W) \times L \times W \times 0.2618$, as previously reported (40).

X-ray examination

The formation of osteolytic lesions was monitored using radiography (FUJIFILM IXFR film; FUJIFILM Co.) and an X-ray system (SOFTEX TYPE CMB; SOFTEX Co.).

Histopathologic analysis

Tumors were fixed in 10% neutralized formalin and embedded in paraffin blocks. Sections were stained with hematoxylin/eosin (H&E) and analyzed by light microscopy.

Statistical analysis

Data are expressed as means ± SD. Student's t test was used to compare differences between groups. Pearson's product–moment correlation coefficients were calculated using PASW statistics version 18 software (SPSS Inc.). Statistical significance was defined when the P value was less than 0.05.

Results

In vitro cytopathic efficacy of OBP-301 against human bone and soft tissue sarcoma cell lines

To evaluate the *in vitro* cytopathic effect of OBP-301 against nonepithelial malignant cells, 14 tumor cell lines

Published OnlineFirst February 16, 2011; DOI:10.1158/1078-0432.CCR-10-2066

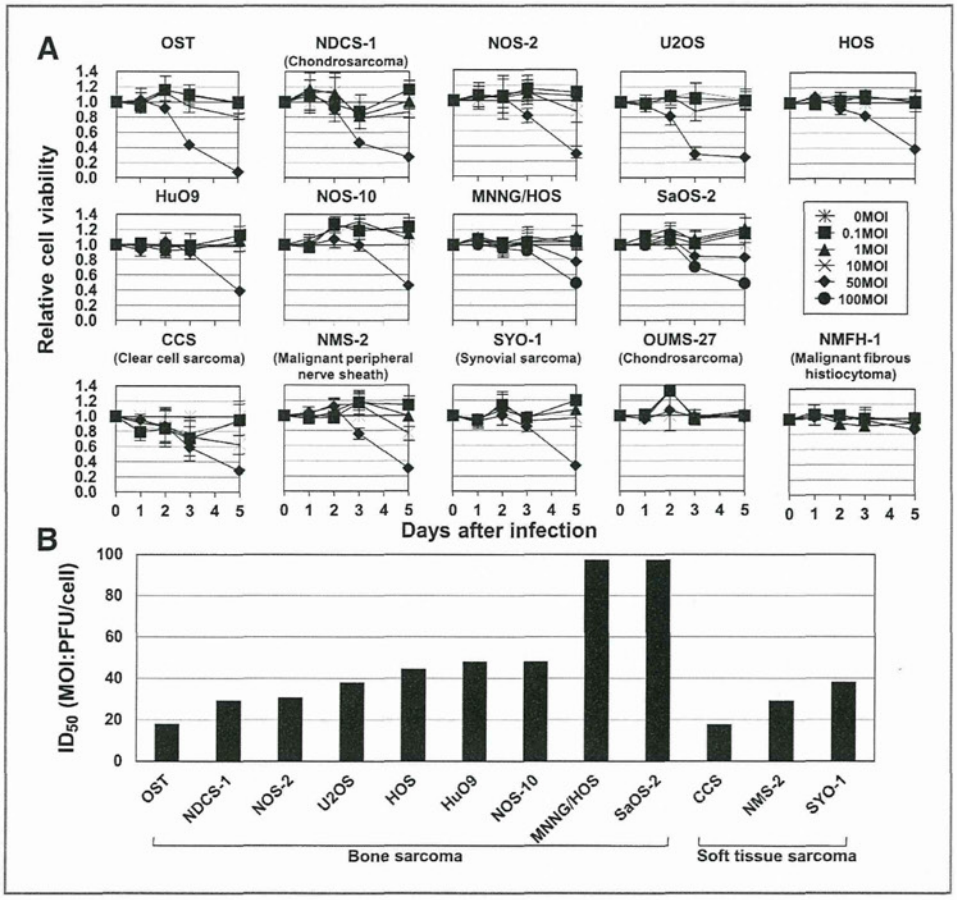

Figure 1. Cytopathic effect of OBP-301 on human bone and soft tissue sarcoma cell lines. A, cells were infected with OBP-301 at the indicated MOI, and cell survival was quantified over 5 days using the XTT assay. The cell viability of mock-treated group on each day was considered 1.0, and the relative cell viability was calculated. Data are means ± SD. The types of tumor except for osteosarcoma were shown in parentheses. B, the 50% inhibiting doses of OBP-301 on cell viability 5 days after infection were calculated and are expressed as ID_{50} values.

derived from human bone and soft tissue sarcomas were infected with various doses of OBP-301. The cell viability of each cell line was assessed over 5 days after infection by the XTT assay. OBP-301 infection induced cell death in a time-dependent manner in all sarcoma cell lines except for the OUMS-27 and NMFH-1 cell lines (Fig. 1A). Calculation of the ID_{50} values revealed that, of the 12 OBP-301–sensitive sarcoma cell lines, MNNG/HOS and SaOS-2 cells were relatively less sensitive than the other 10 sarcoma cell lines (Fig. 1B). Furthermore, to rule out the possibility that cytopathic effect of OBP-301 is due to nonspecific toxicity based on the high uptake of virus particles into tumor cells, we examined the cytopathic activity of replication-deficient dl312 in U2OS and HOS cells. dl312 did not show any cytopathic effect in U2OS and HOS cells, even when these cells were infected with dl312 at high dose (50 and 100 MOIs; Supplementary Fig. S1). These results indicate that OBP-301 is cytopathic for most human bone and soft tissue sarcoma cells line but that some sarcoma cell lines are resistant to OBP-301.

Expressions of the adenovirus receptor and *hTERT* mRNA on human bone and soft tissue sarcoma cell lines

Because adenovirus infection efficiency depends mainly on cellular CAR expression (22), we determined the expression level of CAR on the 14 sarcoma cell lines by flow cytometry. The 12 OBP-301–sensitive sarcoma cell lines showed CAR expression, determined as MFIs, at various levels, whereas the OBP-301–resistant OUMS-27 and NMFH-1 cells did not express CAR (Fig. 2A and Supplementary Fig. S2).

OBP-301 contains the *hTERT* gene promoter, which allows it to tumor specifically regulate the gene expression of *E1A* and *E1B* for viral replication. Thus, OBP-301 can efficiently replicate in human cancer cells with high telomerase activity but not in normal cells without telomerase activity (12). Recently, some populations of human sarcoma cells have been shown to possess low telomerase activity and to maintain telomere lengths through an ALT mechanism (17–19). Thus, it is probable that OBP-301 cannot efficiently replicate in, and kill, ALT-type human sarcoma cells because of their low telomerase activity. To assess whether the telomerase activity of human sarcoma cells affects the cytopathic activity of OBP-301, we analyzed *hTERT* mRNA expression levels in the 14 sarcoma cell lines by quantitative real-time reverse transcriptase PCR (RT-PCR) analysis. Thirteen of the sarcoma cell lines had detectable *hTERT* mRNA expression at variable levels, and only SaOS-2 cells did not express *hTERT* mRNA (Fig. 2B).

Published OnlineFirst February 16, 2011; DOI:10.1158/1078-0432.CCR-10-2066

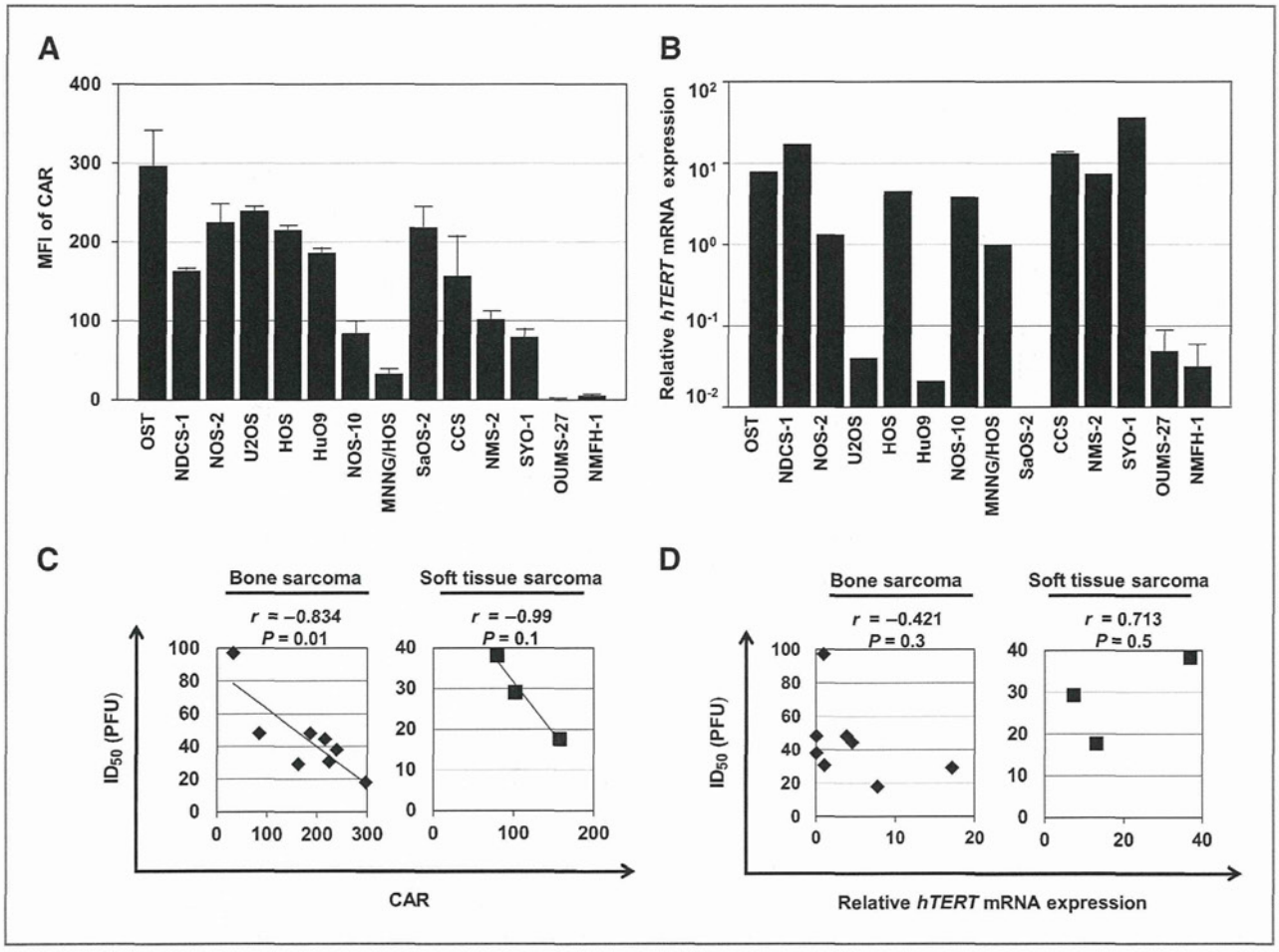

Figure 2. Relationship between the expression levels of CAR and *hTERT* mRNA and the cytopathic activity of OBP-301 against human bone and soft tissue sarcoma cell lines. A, the MFI of CAR expression on human bone and soft tissue sarcoma cells. The cells were incubated with a monoclonal anti-CAR (RmcB) antibody, followed by flow cytometric detection using an FITC-labeled secondary antibody. B, expression of *hTERT* mRNA in human bone and soft tissue sarcoma cells by quantitative real-time PCR. The relative levels of *hTERT* mRNA were calculated after normalization with reference to the expression of *GAPDH* mRNA. C, correlation between the MFI of CAR and the ID_{50} of OBP-301 on human bone and soft tissue sarcoma cells. D, correlation between *hTERT* mRNA expression and the ID_{50} of OBP-301 on human bone and soft tissue sarcoma cells. Statistical significance was determined as $P < 0.05$, after analysis of Pearson's correlation coefficient.

We next investigated the relationship between CAR and *hTERT* mRNA expressions and the cytopathic activity of OBP-301 among the 11 CAR-positive sarcoma cell lines with *hTERT* gene expression. CAR expression levels significantly ($r = -0.834$; $P = 0.01$) correlated with the cytopathic activity of OBP-301 against 8 of the bone sarcoma cell lines (Fig. 2C). CAR expression in 3 of the soft tissue sarcoma cell lines also correlated ($r = -0.99$) with the cytopathic effect of OBP-301, but the differences did not reach significance ($P = 0.1$) because of the low number of cell lines assayed. In contrast, there was no significant correlation between *hTERT* mRNA expression and the cytopathic activity of OBP-301 (Fig. 2D). These results indicate that the cytopathic activity of OBP-301, at least in part, depends on CAR expression.

Furthermore, SaOS-2 and U2OS cells have already been shown to be ALT-type sarcoma cell lines with low telomerase activity (9, 17). Among these ALT-type sarcoma cells, U2OS cells showed a sensitivity to OBP-301 that was similar to that of non–ALT-type sarcoma cells such as HOS and NOS-10 (Fig. 1B). These results indicate that ALT-type human sarcoma cells are sensitive to OBP-301 and that a low telomerase activity does not detract from the cytopathic activity of OBP-301.

Enhanced virus replication and cytopathic activity of OBP-301 through *hTERT* mRNA upregulation in ALT-type sarcoma cell lines

The high sensitivity of ALT-type sarcoma cells to OBP-301 prompted us to hypothesize that OBP-301 may activate the *hTERT* gene promoter, thereby enhancing the viral replication rate and subsequently inducing cytopathic activity in ALT-type sarcoma cells. Furthermore, it has been previously shown that the adenoviral E1A

Published OnlineFirst February 16, 2011; DOI:10.1158/1078-0432.CCR-10-2066

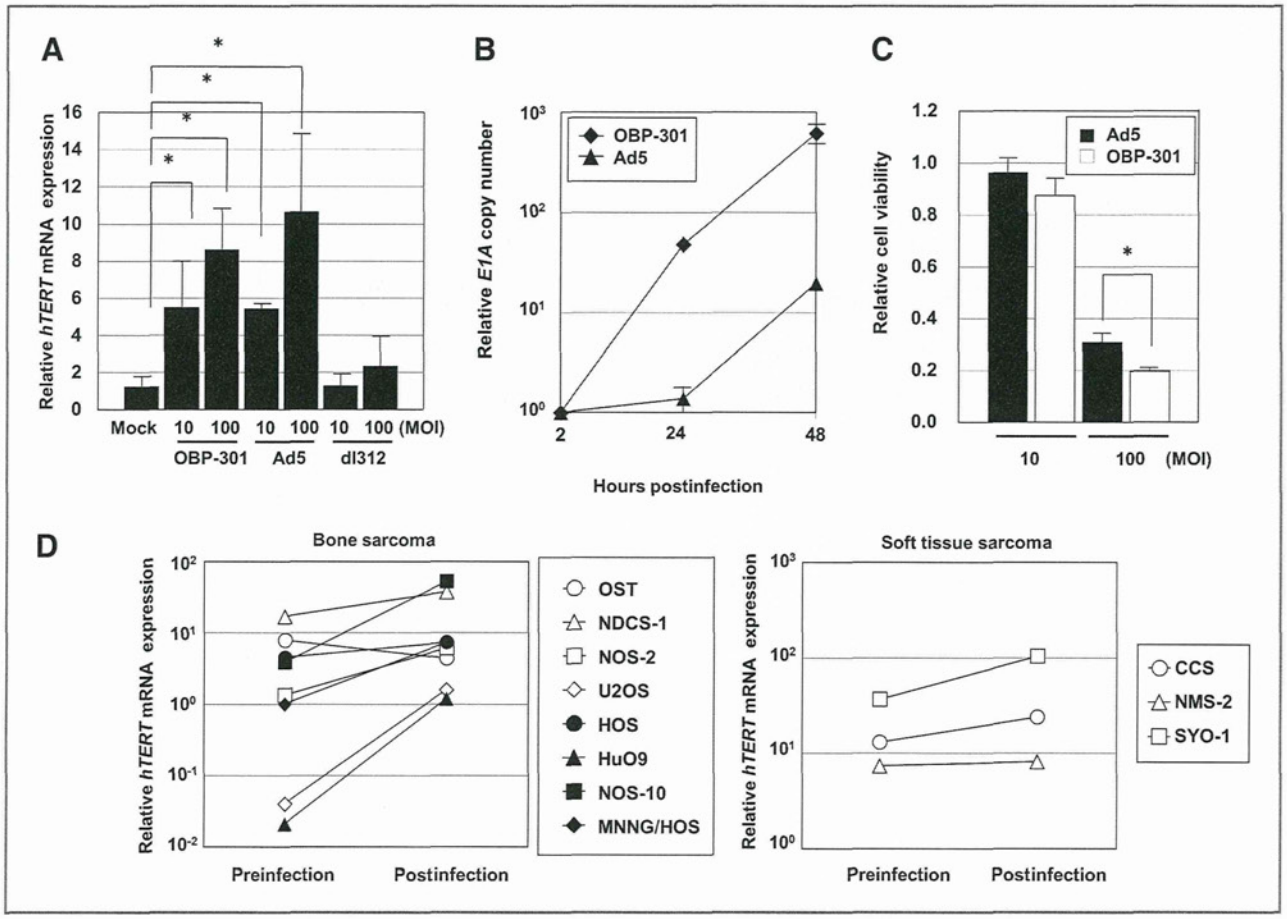

Figure 3. Upregulation of *hTERT* gene expression in ALT-type human sarcoma cell lines enhances the replication and the cytopathic effect of OBP-301. A, expression of *hTERT* mRNA in U2OS cells that were mock-infected or were infected with OBP-301, Ad5, or dl312. The cells were infected with OBP-301, Ad5, or dl312 at the indicated MOIs for 48 hour, and *hTERT* mRNA expression was analyzed using quantitative real-time RT-PCR. The value of *hTERT* mRNA expression in the mock-infected cells was set at 1, and relative mRNA levels were plotted. B, quantitative measurement of viral DNA replication in U2OS cells infected with OBP-301 or Ad5. The cells were infected with OBP-301 or Ad5 at an MOI of 10 PFUs/cell, and *E1A* copy number was analyzed over the following 2 days by quantitative real-time PCR. The value of the *E1A* copy number at 2 hours after infection was set at 1, and relative copy numbers were plotted. C, comparison of the cytopathic effect of OBP-301 and Ad5 in U2OS cells. The cells were infected with OBP-301 or Ad5 at the indicated MOIs, and cell survival was quantified 5 days after infection by using an XTT assay. D, expression of *hTERT* mRNA after infection of human bone (left) and soft tissue (right) sarcoma cell lines with OBP-301 at an MOI of 100 PFUs/cell. Statistical significance (*) was determined as $P < 0.05$ (Student's t test).

protein can activate the promoter activity of the *hTERT* gene (41, 42). Therefore, to determine whether OBP-301 infection activates *hTERT* mRNA expression, we examined the expression level of *hTERT* mRNA in ALT-type U2OS cells after infection with OBP-301 at MOIs of 10 and 100 PFUs/cell (Fig. 3A). Compared with mock-infected U2OS cells, OBP-301–infected U2OS cells showed a 6- to 8-fold increase in *hTERT* mRNA expression in a dose-dependent manner. Ad5 infection also increased *hTERT* mRNA expression in U2OS cells, whereas there was no increase in U2OS cells infected with *E1A*-deleted dl312. These results suggest that OBP-301 is cytopathic for ALT-type sarcoma cells through E1A-mediated activation of the *hTERT* gene promoter.

We next compared viral replication rates after infection of ALT-type U2OS cells with OBP-301 or Ad5. As expected, the viral replication rate of OBP-301 was significantly higher than that of Ad5 (Fig. 3B). Furthermore, the cytopathic activity of OBP-301 was significantly higher than that of Ad5 against the ALT-type U2OS cells (Fig. 3C). Finally, to determine whether OBP-301 activates *hTERT* mRNA expression in both ALT-type and non–ALT-type human sarcoma cell lines, we infected 11 CAR-positive human sarcoma cells with OBP-301 at 100 MOI. Ten of the 11 CAR-positive human sarcoma cell lines showed an increase in the expression level of *hTERT* mRNA after OBP-301 infection that ranged from a 1.1- to 50.0-fold increase (Fig. 3D and Supplementary Table S1). In addition, the expression level of *hTERT* mRNA was also upregulated when OST cells were infected with 5 or 50 MOI of OBP-301 (Supplementary Fig. S3). These results suggest that OBP-301 is cytopathic for both ALT-type and non–ALT-type human sarcoma cells through activation of the *hTERT* gene promoter.

Published OnlineFirst February 16, 2011; DOI:10.1158/1078-0432.CCR-10-2066

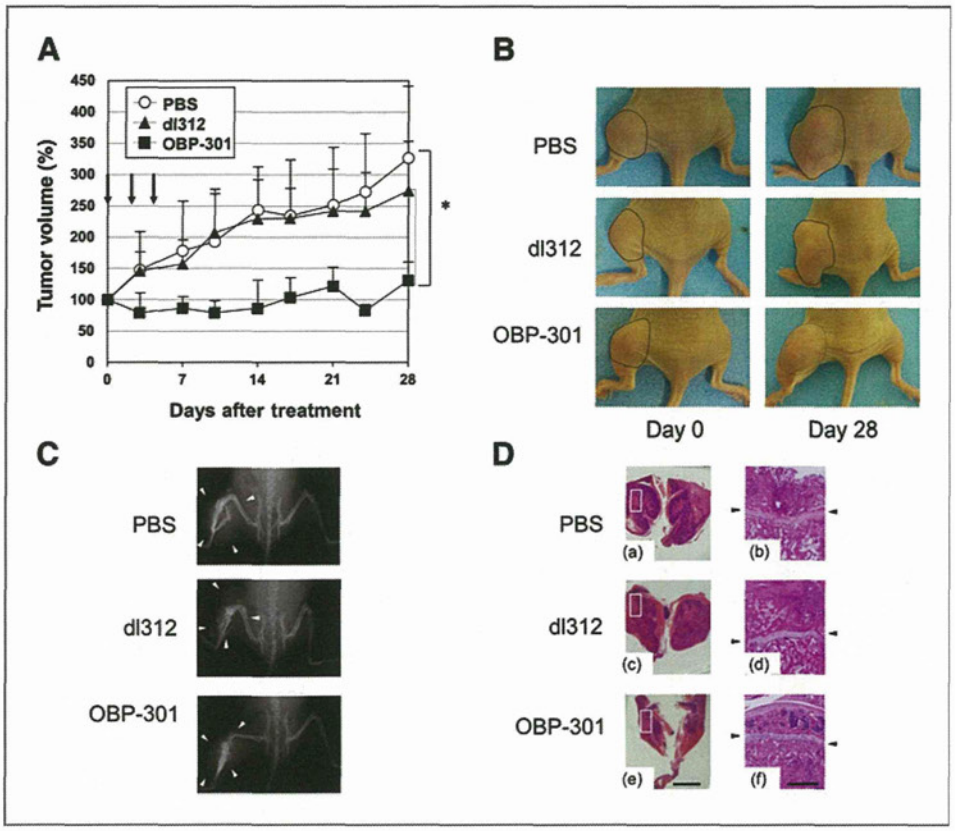

Figure 4. Antitumor effect of OBP-301 in an orthotopic OST bone sarcoma xenograft model. A, athymic nude mice were inoculated intratibially with OST cells (5×10^6 cells/site). Fourteen days after inoculation (designated as day 0), OBP-301 (■) or OBP-405 (▲) was injected into the tumor, with 1×10^8 PFUs on days 0, 2, and 4. PBS (○) was used as a control. Four mice were used for each group. Tumor growth was expressed as mean tumor volume ± SD. Statistical significance (*) was determined as $P < 0.05$ (Student's t test). B, macroscopic appearance of OST tumors in nude mice on days 0 and 28 after treatment with PBS, dl312, or OBP-301. Tumor masses are outlined by a dotted line. C, X-ray photographs of mice bearing OST tumors. The white arrowheads indicate the space occupied by the tumor mass. D, histologic analysis of the OST tumors. Tumor sections were obtained 28 days after inoculation of tumor cells. Paraffin-embedded sections of OST tumors were stained with H&E. The black arrowheads indicate growth plate cartilages. a, c and e, are low-magnification images and b, d and f are high-magnification images of the area outlined by a white square. Left scale bar, 5 mm. Right scale bar, 500 μm.

Antitumor effect of OBP-301 against 2 orthotopic tumor xenograft models

To evaluate the *in vivo* antitumor effect of OBP-301 against human bone and soft tissue sarcomas, we used 2 types of orthotopic tumor xenograft models: the OST bone sarcoma xenograft and the SYO-1 subcutaneous soft tissue sarcoma xenograft. We first identified a dose of OBP-301 that was suitable for induction of an antitumor effect in the subcutaneous OST bone sarcoma xenograft model (determined as $>10^7$ PFUs; Supplementary Fig. S4). We next assessed the antitumor effect of OBP-301 on the orthotopic OST bone sarcoma xenograft model. OBP-301 was injected into the tumor once a day for 3 days, with 10^8 PFUs per day (10). Replication-deficient adenovirus dl312 or PBS was also injected into control groups. Tumor growth was significantly suppressed by OBP-301 injection compared with injection of dl312 or PBS (Fig. 4A). Macroscopic analysis of the tumors indicated that OBP-301–treated tumors were consistently smaller than dl312- or PBS-treated tumors on day 28 after treatment (Fig 4B). We further determined whether OBP-301–treated tumors were less destructive to surrounding normal tissues than control tumors, using X-ray and histologic analyses (Fig. 4C and D). X-ray examination revealed that OBP-301–treated tumors resulted in less bone destruction than dl312- or PBS-treated tumors. Histologic findings were consistent with the X-ray results, showing that some tumor tissue had penetrated over the growth plate cartilage in dl312- and PBS-treated tumors but not in OBP-301–treated tumors.

With future clinical application in mind, we sought to establish a suitable protocol for repeated intratumoral injection of OBP-301 by using an orthotopic SYO-1 soft tissue sarcoma xenograft model. Doses of OBP-301 that were suitable for induction of an antitumor effect on SYO-1 tumors ($>10^8$ PFUs) were determined in a manner similar to that of OST bone sarcoma cells (data not shown). OBP-301 was injected 3 times into the tumor, with 10^9 PFUs and intervals of 1 day, 2 days, or 1 week between injections (Supplementary Fig. S5). A total of 3 OBP-301 injections, with intervals of 2 days or 1 week between injections, induced a significant